Gas phase molecular relaxation probed by synchrotron radiation experiments

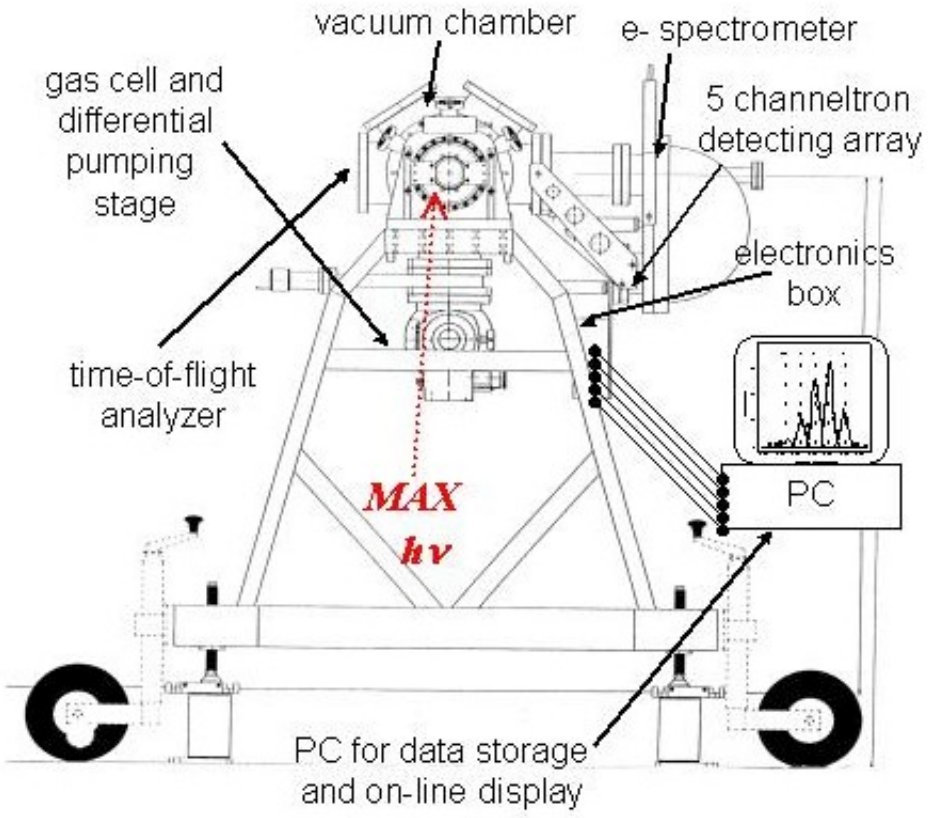

Jaume Rius i Riu

Royal Institute of Technology (KTH), Section of Atomic and Molecular Physics, Albanova, Stockholm, 2002

TRITA-FYS-2002:32
ISSN 0280-316X
ISRN KTH/FYS/--02:32—SE

Gas phase molecular relaxation probed by synchrotron radiation experiments

Jaume Rius i Riu
Royal Institute of Technology (KTH), Section of Atomic and Molecular Physics, Albanova, Stockholm, October 2002

Abstract

This thesis presents experimental studies of gas phase molecular relaxation after excitation with synchrotron photons in the 15-35 eV and in the 70-350 eV regions.

In the 15-35 eV region, molecular relaxation by neutral dissociation processes and non Franck-Condon effects in N_2 and O_2 molecules have been studied by means of dispersed fluorescence and photoelectron spectroscopy experimental techniques, respectively. From the dispersed fluorescence data, excitation functions for the measured atomic fluorescence spectra have been obtained. From the recorded photoelectron spectra vibrational branching ratios have been produced. The results obtained reveal that Rydberg series and singly and doubly excited valence states of the appropriate symmetry energetically accessible in the studied region and interactions between them account for most of the observed effects in these two type of experiments.

In the 70-350 eV range, molecular relaxation processes resulting in fragmentation of CD_4 and SF_6 after absorption of synchrotron light have been studied by energy resolved electron ion coincidence technique using a multicoincidence experimental station developed by our group during the last five years for such type of experiments. The coincidence measurements yielded mass spectra from which information about the kinematics of the detected fragments has been deduced by means of Monte Carlo simulations of the experimental peak shapes. The obtained results show completely different dissociation patterns depending on the molecular electronic states studied. These patterns reflect the bonding properties of the excited orbitals and they permit the description and in some cases the identification of the different molecular relaxation pathways observed. The achievements presented in this thesis exemplify the potential of the multicoincidence station used in the reported experiments.

A la jefa i el jefe, a les meves germanes, germans... i respectius, i a tu, Jim! ...i a la resta de familia i d'amics

A Na Gaia

"…caminante no hay camino, se hace camino al andar…"
("…walker there is no path, one makes it by walking…")
A. Machado

Contents

Preface

A team effort has been necessary to achieve the results presented in this thesis. Therefore, first of all, I shall introduce the members of the team that has made possible this work.

Team:
J. Álvarez Ruiz, P. Erman, A. Karawajczyk, A. Kivimäki, E. Melero García, E. Rachlew-Källne, K. Yoshiki Franzén (Stockholm). M. Stankiewicz, P. Winiarczyk (Krakow). S. Aksela, M. Huttula, E. Kukk (Oulu). L. Veseth (Oslo) and P. Hatherly (Reading).

This doctoral thesis is based on research carried out under the period February 1998-August 2002 at the Section of Atomic and Molecular Physics at the Royal Institute of Technology. The thesis main objective is to present the performed work in a clear and self-explanatory manner. I sincerely hope the thesis main goal is achieved entirely throughout. However, I apologize to the reader in advance for any inappropriate or misleading explanation there might be.

This thesis consists of an introductory part and eight scientific papers. The introductory part contains four chapters. Chapter 1 is an introduction to the research performed and its significance within the atomic and molecular physics research field and its influence in other areas of scientific knowledge. Chapter 2 contains a summary of the main theoretical background involved in the present experiments and a summary of the methods used for our computations. Chapter 3 describes the synchrotron radiation source used to implement the experiments. Besides, it describes the experimental detection and data analysis techniques used during the experiments. Finally, chapter 4 provides highlights of the main obtained results.

Jaume Rius i Riu
August 2002

List of publications included in this thesis

The scientific basis of this thesis is contained in the following eight papers:

I P. Erman, A. Karawajczyk, E. Rachlew-Källne, J. Rius i Riu, M. Stankiewicz, K. Yoshiki Franzén and L. Veseth. *Neutral dissociation by non-Rydberg doubly excited states.* Phys. Rev. A **60**, (1999) 426-430.

II A. Karawajczyk, P. Erman, E. Rachlew-Källne, J. Rius i Riu, M. Stankiewicz, K. Yoshiki Franzén and L. Veseth. *Neutral fragmentation of superexcited oxygen molecules.* Phys. Rev. A **61,** (2000) 032718.

III J. Rius i Riu, A. Karawajczyk, M. Stankiewicz, K. Yoshiki Franzén, P. Winiarczyk and L. Veseth. *Non Franck-Condon effects in the ionization of molecular oxygen to the O_2^+ $X\ ^2\Pi_g$ state in the 19-31 eV photon energy region.* Chem. Phys. Lett. **333**, (2001) 91-95.

IV J. Rius i Riu, A. Karawajczyk, M. Stankiewicz, K. Yoshiki Franzén, P. Winiarczyk and L. Veseth. *Non Franck-Condon effects in the ionization of N_2^+ $A\ ^2\Pi_u$ state in the 19-34 eV photon energy region.* Chem. Phys. Lett. **338**, (2001) 285-290.

V M. Stankiewicz, J. Rius i Riu, P. Winiarczyk, J. Álvarez Ruiz, P. Erman, P. Hatherly, M. Huttula, A. Karawajczyk, E. Kukk and E. Rachlew-Källne. *Selective fragmentation of valence and core electron excited CD_4 and SF_6 molecules.* Surf. Rev. Lett. **9**, (2002) 117-123.

VI E. Kukk, J. Rius i Riu, M. Stankiewicz, P. Hatherly, P. Erman, E. Rachlew-Källne, P. Winiarczyk, M. Huttula and S. Aksela. *Dissociation of deuteromethane following carbon 1s core ionization.* Phys. Rev. A. **66**, (2002) 012704.

VII M. Stankiewicz, J. Rius i Riu, P. Winiarczyk, P. Erman, P. Hatherly and E. Rachlew-Källne. *Fragmentation of the SF_6 molecule viewed by energy resolved electron ion coincidence (EREICO) technique using 100 eV synchrotron photons.* Submitted to Chem. Phys. Lett. (2002).

VIII J. Rius i Riu, E. Melero García, J. Álvarez Ruiz, P. Erman, P. Hatherly, E. Rachlew-Källne, M. Stankiewicz and P. Winiarczyk. *Core excitation induced dissociation in CD_4 after participator Auger decay.* Submitted to Phys. Rev. A (2002).

My contribution to these papers always lies in the experimental and data analysis side. I have been actively involved in all experimental sessions during which the data were acquired. L. Veseth has developed all theoretical computations presented in the first four papers. E. Kukk performed the Dalton computations and the following discussion presented in paper VI.

My contribution to papers I and II covers the performance of the data analysis and the preparation of figures 2 and 3 in paper I and figures 1, 3 and 4 in paper II.

Papers III, IV and V have been written by me after discussion of the papers' contents and structure with the rest of the co-authors.

My contribution to paper VI is the performance of the data analysis and simulation work necessary to obtain the results presented in figure 3 and the corresponding discussion of these partial results and their role in the paper's frame with the principal author of the paper, E. Kukk.

Paper VII and paper VIII have been written by me together with M. Stankiewicz and with E. Melero García, respectively. My contribution to both of them involves the performance of the data analysis and structuring the results presented after discussing them with the co-authors.

Other publications not included in this thesis

I M. K. Thomas, P. A. Hatherly, K. Codling, M. Stankiewicz, J. Rius i Riu, A. Karawajczyk and M. Roper. *Soft x-ray ionization and fragmentation of n- and iso-propanol.* J. Phys. B: At. Mol. Opt. Phys. **31**, (1998) 3407-3418.

II E. Rozan, C. Collado, A. Garcia, J. M. O'Callaghan, R. Pous, L. Fabrega, J. Rius i Riu, R. Rubí, J. Fontcuberta and F. Harackiewicz. *Design and fabrication of coplanar YBCO structures on lithium niobate substrates.* IEEE-Transactions-on-Applied-Superconductivity **9,** (1999) 2866-2869.

III P. Erman, A. Karawajczyk, E. Rachlew-Källne, J. Rius i Riu, M. Stankiewicz, K. Yoshiki Franzén, A. Weider Moen and L. Veseth. *Non Franck-Condon effects in photoionization of molecular oxygen.* Physica Scripta **62,** (2000) 294-300.

IV J. Rius i Riu, A. Karawajczyk, M. Stankiewicz and P. Winiarczyk. *A position sensitive time-of-flight analyser for study of molecular photofragmentation.* Nucl. Instr. and Meth. A **477**, (2002) 360-364.

V P. A. Hatherly, J. Rius i Riu, M. Stankiewicz, F. M. Quinn and L. J. Frasinski *Dynamics of the shake-up satellites of C 1s excited carbon dioxide studied by threshold electron spectroscopy.* J. Phys. B: At. Mol. Opt. Phys. **35**, (2002) L77-L83.

VI J. Rius i Riu, J. Álvarez Ruiz, A. Karawajczyk, M. Stankiewicz, P. Winiarczyk and L. Veseth. *Non Franck-Condon effects in the photoionization of N_2 to the N_2^+ $A\,^2\Pi_u$ state and of O_2 to the O_2^+ $X\,^2\Pi_g$ state in the 19-34 eV photon energy region.* Surf. Rev. Lett. **9**, (2002) 147-152.

VII J. Álvarez Ruiz, P. Erman, E. Rachlew-Källne, J. Rius i Riu, M. Stankiewicz and L. Veseth. *Neutral fragmentation of superexcited states in CO.* J. Phys. B: At. Mol. Op. Phys. **35**, (2002). 2975-2983.

VIII M. Stankiewicz, J. Rius i Riu, A. Karawajczyk and J.O. Forsell. *A new experimental station for angular-resolved coincidence measurements with energy-resolved electrons.* Manuscript to be published.

Acknowledgments

I want to start by thanking Prof. P. Erman, Prof. E. Rachlew and Dr. A. Karawajczyk for making it possible for me to come to The Royal Institute of Technology, Physics I department and become a member of the Atomic and Molecular Physics group. Also I thank them for their support throughout the time required for me to get my PhD.

I admire and thank Prof. Marek Stankiewicz at the Jagiellonian University in Krakow, Poland, for guiding me through this exciting and complex world of science and technology. And for having the patience and energy to put up with me throughout these years even if I am no match for him in the tennis court! Marek, I just wish my *processor* learns to work as fast as yours so I can entertain you a bit one day… And not just learn from you as up to now. And many thanks to your wonderful family for their love while my stay in Krakow I do not forget them. Also at the Jagiellonian University I want to send many thanks to Piotr Winiarczyk for his help and his excellent program to simulate the mass spectra peak shapes.

I thank to Doc. P. A. Hatherly for accepting me under his supervision while I was an Erasmus student in Reading University, UK. He introduced me to the fascinating world of Atomic and Molecular Physics and Synchrotron radiation. Paul, you are the ulterior reason that allowed me to be here today. Thank you for your trust and confidence on me. I hope to deserve it for years to come...

It has been a great luck for me to collaborate with the photoelectron spectroscopy group at Oulu University, Finland. Specially rewarding has been the contribution from Edwin Kukk and Marko Huttula during the experimental beam times we shared. Also, it has been a pleasure to participate in the nice work that Edwin has performed on paper VI. I also want to thank Helena and Seppo Aksela, Anna and Saana and the rest of the group for their hospitality and help during my stays among them.

I warmly thank Prof. Leif Veseth from Oslo University, Norway, for his help, patience and understanding when explaining to me the details of his computations and of the many-body perturbation theory. I hope the theoretical part of this thesis does not disappoint you, Leif!

I owe to Ken Yoshiki Franzén not only what I know about the experiments we have performed together, but all what I was able to experience and enjoy in my first year. And understand me; what we enjoyed did not just happen in the lab, there were some parties and adventures that I will never forget… Thank you from my heart, Ken. I also want to thank you and Madoka for making me feel your warmth and care while my stay in Tokyo during your wedding. Thanks!

I also want to thank all the people related with this thesis I have had the chance to work with. I hope I do not forget anyone. At Physics I, many thanks to Agneta Falk, Rune Persson, Prof. S. Stenholm, Prof. L.-E. Berg, Prof. R. Wyss, Tony Hanson, P. v d Meulen, Renée Andersson *angelito mío…* Katrin Ekvall, Cecilia, Niklas, Bo, Anders, Bob, Marika, Ming and Erika. I thank Ahmed, Cristina and Joseph Al-Khalili for being as they are and allowing me to enjoy being their friend. I also want to thank Stefan, Marie, Anita, Jacek and Richard for all the nice evenings of recreation… In MAX LAB I am indebted with all the scientific, engineering and administrative staff. They perform the great job that allows us to go there and perform such nice experiments as the ones presented here. Specially, thank you, Helena, for always having a smile and a song for us. You are HAPPINESS itself! And thanks to the De Dios-Sabarich family for coming all the way from Lleida, twice, (8000 km, return) to visit me… with the kids and the grandpa in a motor home! I love you!

Thanks to my family in Stockholm; they are as essential to me as the air I breathe. They are of course Jesús and Emilio; your presence here changed my life completely. You are ******* good, guys! THANK YOU BOTH! And many thanks also to their respective families... And Monica and Ulf. And during their time here, all the Erik-sons and daughters; Mamen, Nuria, Gemma, Carlos and specially Isabel; she taught me how to learn more about myself and therefore how to be happier in life… you gave me more than you know, Isa. *Gracias con todo mi corazón Isabel*. Also they are part of the family now and forever Peio, and Bea and *sus dos gordos, Alex y Alba… sí, familia, eh, Bea!* Also Carlos, José, Toni, Raul and Helena and their families helped me to be happy in Stockholm. They have the best *tapas* restaurant, Olé Olé, in Hantverkargatan 32, Stockholm …my second home!

And of course here I want to say,

TO MY FAMILY
I have a great family that has been there for me,
every single time I needed them,
in every occasion, during all my life!
I am a very lucky person for that.
I am the way I am because them
…and for them. I love them all very much…

Per això aquest poema es per a vosaltres:

Estava espantat i suat. I cridant. I plorant
Preocupat i angoixat. I ofegant-me... Estava dormint, somiant!
En despertar-me, allà estàveu tots.
Junts, rient i plorant. I cantant. I ballant.
I celebrant i barallant-nos. I sent feliços... Estava a casa, dinant!

I despert m'adono que casa és a Lleida, i a La Bordeta, i a
Barcelona, i a Granollers, i a Tenerife... I a Mallorca,
i a Whistable i a Estocolm... i fins i tot a Donosti i a Dubai!
Casa es allà on estiguem cadascun de nosaltres, família...
només cal el nostre amor per tenir-nos a tots, de cop, a l'instant

Aquest amor és la nostra riquesa i la nostra força.
És el més gran regal que ens podem donar.. i ens fa especials.
I cal que el treballem, dia a dia, hora a hora, com fem...
Per a poder-lo assaborir i gaudir, entre tots, de veritat...

És també l'ensenyament més important per als joves de casa,
Com un cop a nosaltres nostres pares ens ho van ensenyar...
Ensenyem-los doncs a sentir l'amor i treballar per mantenir-lo,
I podran ser feliços, amb patiment... però amb l'amor més gran.
Us estimo família.

TO MERCEDES
Quiero agradecer al destino, Mercedes,
que nos hayamos conocido y hayamos coincidido...
...así como le agradezco, Mercedes, nuestras vidas hasta ahora,
por juntarnos y permitirnos descubrir y sentir lo que sentimos: FELICIDAD.
Felicidad abrazándonos y sintiéndonos juntos, mirándonos fijamente a los ojos, enamorados...
besándonos y acariciándonos y hablándonos y escuchándonos, amándonos sin tamaño ni límite alguno
...felicidad que bien vale una vida, Mercedes, tú con Arkaitx y yo con vosotros para siempre, estemos o no juntos

Gràcies a tots! **¡Gracias a todos!** **Thanks to you all!** **Tack så mycket till er alla!**

Chapter 1

Introduction

This thesis presents the work developed from February 1998 until August 2002 in the field of experimental atomic and molecular physics. In particular, the experiments described in this thesis deal with the processes taking place on free and non-interacting molecules after photon absorption in the VUV and X-ray regions. The efforts have been focused mainly on experimental studies of molecular relaxation dynamics and molecular structure. Since the basics of this area of knowledge is the interaction between radiation (light) and matter, it plays an important role in the development of fundamental physics and chemistry and consequently, several natural sciences and technology disciplines are directly affected by the progresses achieved in this field. Subjects as diverse as environmental science (for example, ozone formation and dissociation) [1], biological sciences (for example, cockroach reproduction control) [2] or medical, electrical power and aeronautic technologies [3 and references therein] use the fundamental understanding gained by means of atomic and molecular studies of the appropriate systems to continuously increase the knowledge in their own fields.

Half of this thesis is dedicated to investigations of molecular relaxation dynamics and structure of N_2 and O_2 after excitation with VUV photons in the range of 15 to 34 eV. For the past eleven years the group at the atomic and molecular physics department (KTH) has been involved in the study of fragmentation and ionization of small molecules. In particular, experiments on ionization of N_2 molecules to the B state of the N_2^+ ion combined with many-body perturbation theory calculations provided experimental evidence of the existence of Non Rydberg Doubly Excited Resonances (NRDERs) in valence excitation region [4] predicted already in 1979 by G. Wendin [5]. These states are short-lived, with lifetimes of the order of femtoseconds and therefore very difficult to detect experimentally. Conveniently, dispersed fluorescence measurements [6] of vibrationally resolved emission lines of the (1,2) and (0,1) N_2^+ (B-X) transitions produced by absorption of VUV photons yielded the branching ratio spectra which compared with the calculations provided by Prof. L. Veseth allowed the assignment of the experimental features observed as NRDERs, with electron configurations such that favored their autoionization to the B state of the N_2^+ molecular ion. Similar studies have been developed on other diatomic molecules such as CO and NO [7]. Papers I to IV present the efforts carried out by means of dispersed fluorescence and photoelectron spectroscopy experiments, using synchrotron light as excitation source, to achieve a clearer understanding of the molecular structure and relaxation pathways of N_2 and O_2. As it is explained further, excited states of Rydberg and non-Rydberg character play a crucial role in the relaxation of these molecules. A recent

review on the subject reports more experimental evidence of NRDERs after synchrotron excitation [8]. Also, electron-energy-loss spectroscopy [9], asymmetric (e, 2e) experiments [10] and Auger decay measurements of core excited nitrogen atoms [11] inform of the existence of doubly excited states in the corresponding energy regions. Besides the direct application of these results on the development of molecular quantum mechanics and quantum chemistry models, the knowledge gained in these fundamental studies is useful for example in atmospheric science [12], astrophysics [13], condense matter physics [14] and also technological efforts in industry and science as important as the development of X-ray lasers [15].

The second part of this thesis is dedicated to investigations of molecular relaxation dynamics resulting in fragmentation of SF_6 and CD_4 after excitation with synchrotron light in the range of 70 to 350 eV. All the included coincidence experiments use a newly built experimental station for angular-resolved coincidence measurements with energy-resolved electrons, which is described in detail in a forthcoming publication. Chapter 3, however, includes a self-contained and comprehensive description of the station. The design, construction, set up and testing of the station have occupied most of the time of the last five years. The main objective of this experimental station is to allow the study of molecular fragmentation following core or valence ionization correlating energy- (and angular-) resolved electrons and mass-resolved ions in a coincidence experiment, i.e. to permit the *complete* experiments in molecular photoionization [16]. In particular, this thesis presents Energy Resolved Electron Ion COincidence (EREICO) measurements on the SF_6 and CD_4 molecules. This type of experiments have revealed themselves a powerful tool in studies of complex molecular relaxation scenarios such as the effects of nuclear motion in the molecular dissociation after resonant Auger decay in core-excited molecules [17]. Therefore, EREICO measurements of SF_6 can bring new information of great relevance in the field of for instance, environmental protection. The sulfur hexafluoride molecule strongly contributes to the earth's global warm up by greenhouse effect. Therefore, its decomposition needs to be carefully studied, described and understood [18]. Besides, gas phase SF_6 fragmentation studies are relevant directly all the SF_6 plasma technology developed for ultra-large scale etching applications [19]. The deuteromethane molecule, CD_4, is of interest for a large variety of research fields. Among others, photochemistry [20,21], astrophysics [22] and elementary particle physics [23] need of the knowledge gained in molecular relaxation dynamics studies such as those presented in this thesis.

Chapter 2

Theoretical method

All the experiments included in this thesis study the relaxation mechanisms of the excited molecules following photon absorption. Depending on the energy absorbed by the molecules, different relaxation scenarios become possible. The quantum mechanical formulation of the fundamental laws of molecular physics and molecular quantum mechanics involved in the present studies are widely treated in the literature at all levels [24,25,26,27,28,29]. Therefore, they are not extensively discussed in this thesis. Instead, the principles and models describing each of the possible scenarios are summarized.

2.1 The Franck-Condon principle

The main physical principle, common to the N_2 and O_2 studies presented in papers I to IV, is the Franck-Condon principle [30,31]. This principle states that *the electron "jump" in a molecular transition takes place so rapidly in comparison to the vibrational motion of the nuclei that immediately after the electron "jump" the nuclei still have very nearly the same relative position and velocity as before the" jump"* [25]. Thus, when an electronic transition occurs, as the one exemplified in Fig. 1, only vertical jumps can take place between vibrational levels of the two different electronic states represented by the lower and upper potential curves in the figure. Hence, one can assume that within the time in which an electronic transition occurs, the nuclei of the diatomic molecule have

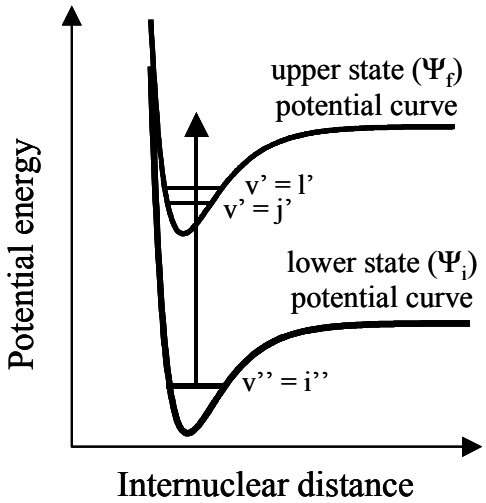

Fig. 1. Transition between two electronic states in a molecule. According to the Franck-Condon principle the transition occurs vertically in the diagram, in the direction indicated by the arrow.

hardly changed their position at all. Thus, if we want to investigate the spectra of a particular electronic transition theoretically, the Franck-Condon principle allows us to separate the wave functions describing the initial (Ψ_i) and final states (Ψ_f) into an electronic wave function, which describes only the electron motion, and a vibrational wave function, which describes just the nuclei vibrational motion.

$$\Psi_i = \Psi_{elec,i}\Psi_{vibr,i} \tag{1}$$

$$\Psi_f = \Psi_{elec,f}\Psi_{vibr,f} \tag{2}$$

There, we neglect rotational motion since it does not change the further consideration. For the same reason, the dipole moment operator $\mathbf{M}$ can be separated into an electronic and a nuclear part as

$$\mathbf{M} = \mathbf{M}_{elec} + \mathbf{M}_{nucl} \tag{3}$$

The transition dipole moment between the initial and final states can then be written as

$$\begin{aligned} \left\langle \Psi_f \left| M \right| \Psi_i \right\rangle &= \left\langle \Psi_{elec,f}\Psi_{vibr,f} \left| \mathbf{M}_{elec} + \mathbf{M}_{nucl} \right| \Psi_{elec,i}\Psi_{vibr,i} \right\rangle = \\ &= \left\langle \Psi_{elec,f}\Psi_{vibr,f} \left| \mathbf{M}_{elec} \right| \Psi_{elec,i}\Psi_{vibr,i} \right\rangle + \left\langle \Psi_{elec,f}\Psi_{vibr,f} \left| \mathbf{M}_{nucl} \right| \Psi_{elec,i}\Psi_{vibr,i} \right\rangle \end{aligned} \tag{4}$$

The second term is zero since the operator $\mathbf{M}_{nucl}$ does not depend on the electronic coordinates leaving the orthogonal wave functions $\Psi_{elec,i}$ and $\Psi_{elec,f}$ unchanged. The remaining first term is

$$\begin{aligned} &\left\langle \Psi_{elec,f}\Psi_{vibr,f} \left| \mathbf{M}_{elec} \right| \Psi_{elec,i}\Psi_{vibr,i} \right\rangle = \\ &= \int \Psi^*_{elec,f} \mathbf{M}_{elec} \Psi_{elec,i} d\tau_{elec} \int \Psi^*_{vibr,f} \Psi_{vibr,i} d\tau_{nucl} \end{aligned} \tag{5}$$

Where $d\tau_{elec}$ and $d\tau_{nucl}$ are the respective volume elements of the space of the electronic and nuclear coordinates. The second integral can assume non-zero values since the vibrational wave functions associated to different electronic states are not orthogonal.

Thus, the emission intensity of an electronic transition between two different states including the vibrations of the nuclei can be expressed as follows [25]

$$\begin{aligned} I^{em}_{v'v''} &\propto \nu^4 \cdot N_{v'} \cdot \left| \int \Psi^*_{elec,f} \mathrm{M}_{elec} \Psi_{elec,i} d\tau_{elec} \right|^2 \left| \int \Psi^*_{vibr,f} \Psi_{vibr,i} d\tau_{nucl} \right|^2 \\ &\propto \nu^4 \cdot N_{v'} \cdot \mathrm{R}_e^2 \cdot \left| \int \Psi^*_{vibr,f} \Psi_{vibr,i} d\tau_{nucl} \right|^2 \end{aligned} \tag{6}$$

Similarly, the absorption intensity can be expressed as [25]

$$I^{abs}_{v'v''} \propto \nu \cdot N_{v''} \cdot \mathrm{R}_e^2 \cdot \left| \int \Psi^*_{vibr,f} \Psi_{vibr,i} d\tau_{nucl} \right|^2 \tag{7}$$

Where ν is the energy difference between the initial and final states expressed in wave number units. $N_{v'}$ and $N_{v''}$ are the upper and final state populations, respectively. $\mathbf{R}_e^2$ is the electronic transition moment for the particular electronic transition studied and the squared integral is the Franck-Condon factor that indicates the overlap between the initial and final vibrational wave functions.

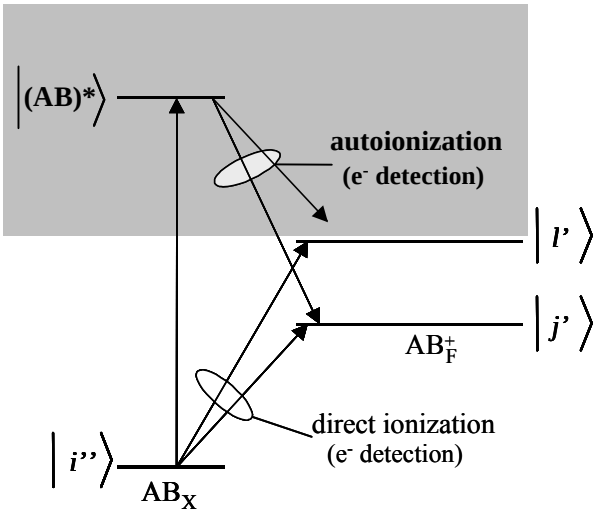

Fig. 2. Schematics of the simultaneous excitation to states AB_F^+ and (AB)*, which leads to deviation of the vibrational populations of $|j'\rangle$ and $|l'\rangle$ achieved if they are populated just by direct ionization. This produces non Franck-Condon effects in the vibrational branching ratios.

Eq. (6) and (7) are a key result to understand the studies presented in papers I to IV. The neutral dissociation studies presented in section 2.2 (papers I and II) are based on the excitation functions of the atomic emission lines observed after synchrotron excitation of O_2 and N_2 molecules. Specifically, paper I presents the relative population of the upper levels of the observed atomic transitions. Paper II presents a slight variation of the excitation function concept, the formation rate functions. The details of the data analysis process to obtain these functions are discussed in section 3.3.1. The non Franck-Condon behavior studies presented in this thesis (papers III and IV) are based on the calculation of the branching ratio between two different vibronic transitions $i'' \rightarrow j'$ and $i'' \rightarrow l'$ as described in section 3.3.2. The branching ratios help to reveal whether a transition between two electronic states of the molecule has taken place directly, involving only the initial and final levels, or if it has involved more intermediate levels, as schematized in Fig. 2, giving rise to so-called non Franck-Condon effects. The theoretical background describing such effects is presented in section 2.1.1 below.

2.1.1 Non Franck-Condon effects

The use of branching ratios measurements combined with theoretical calculations has identified very shortly lived autoionizing states in the case of the N_2 [4,5] and CO molecules [7]. In papers III and IV photoelectron spectroscopy has been used to study the photoionization of N_2 to the N_2^+ A $^2\Pi_u$ state and of O_2 to the O_2^+ X $^2\Pi_g$ state in the 19-34 eV photon energy region. From eq. (7) the branching ratio R of two particular vibronic transitions $i'' \rightarrow j'$ and $i'' \rightarrow l'$ can be obtained as

$$R = \frac{I_{i''\to j'}}{I_{i''\to l'}} \propto \frac{N_{i''} \cdot \mathrm{R}_e^2 \cdot \left|\int \Psi_{j'}^* \Psi_{i''} d\tau_{nucl}\right|^2}{N_{i''} \cdot \mathrm{R}_e^2 \cdot \left|\int \Psi_{l'}^* \Psi_{i''} d\tau_{nucl}\right|^2} \propto \frac{\left|\int \Psi_{j'}^* \Psi_{i''} d\tau_{nucl}\right|^2}{\left|\int \Psi_{l'}^* \Psi_{i''} d\tau_{nucl}\right|^2} \quad (8)$$

R is a value proportional to the overlap integral between the two vibrational states of the two electronic states involved in the transition. The function R is almost constant with the excitation energy for a specific initial vibronic state $|i''\rangle$ of AB_X; i.e. as long as the transitions between *i''*→*j'* and *i''*→ *l'* occur directly [30,31]. However, if a third state is involved in the transition, large deviations from the Franck-Condon level predicted by eq. (8) might appear at the excitation energies where this third state is resonantly accessible, as schematized in Fig. 2. At these energies, the state (AB)* might be populated. Therefore, it can rapidly autoionize to the states $|l'\rangle$ and $|j'\rangle$ contributing to the population of these states together with the direct ionization process populating them simultaneously. Thus, the population of these vibrational levels differs in this case from when they are populated only through direct ionization from AB_X to AB_F^+. These variations of the population are reflected in the experimentally measured vibrational branching ratios as structures around the constant Franck-Condon level of a given transition; i.e. as non Franck-Condon effects. This is the theoretical basis of the discussion contained in papers III and IV.

2.2 Neutral dissociation

Neutral dissociation of a diatomic molecule can occur when the molecule absorbs a photon and instead of ejecting an electron (autoionization), it reaches an excited state that makes the molecule to break into two neutral atomic fragments (predissociation) [24]. These two processes might also occur at the same time since autoionization takes place in time scales around 10^{-12} to 10^{-16} seconds whereas predissociation occurs for time scales shorter than 10^{-13} seconds. This subject has extensively been reviewed [24] and therefore this section describes exclusively the parts directly related to the studies performed in papers I and II. There, dispersed fluorescence from excited atomic N and O fragments respectively has been measured. The atomic emission has been studied as a function of the excitation energy by means of excitation functions of the upper atomic states involved in the observed emissions. The neutral fragmentation process studied in papers I and II can be formulated as follows:

$$AB_X + h\nu \quad \rightarrow \quad (AB)^* \quad \rightarrow \quad A^* + B \quad (9)$$

Where AB_X is the molecule in its ground state, (AB)* is the molecule in an excited state and A* is the excited atomic fragment that fluoresces and B is the second atomic fragment in the ground state. The situation described above can be represented in terms of the potential curves of the states involved (Fig. 3). The molecule absorbs a photon and the electron transition takes the molecule from the ground state AB_X to the ionic state I by crossing it at **a** or to the excited state (AB)* by crossing at **b**. At the crossing point **a,** the molecule is still within the well of the molecular ionic state I and since the crossing point **a** is lying higher up than the dissociation limit for (AB)* it can lead to dissociation at the limit **c** through curve crossing between I and (AB)*. At the crossing point **b** the molecule is clearly above the well of the molecular state (AB)* and dissociation at the limit **c** is also possible.

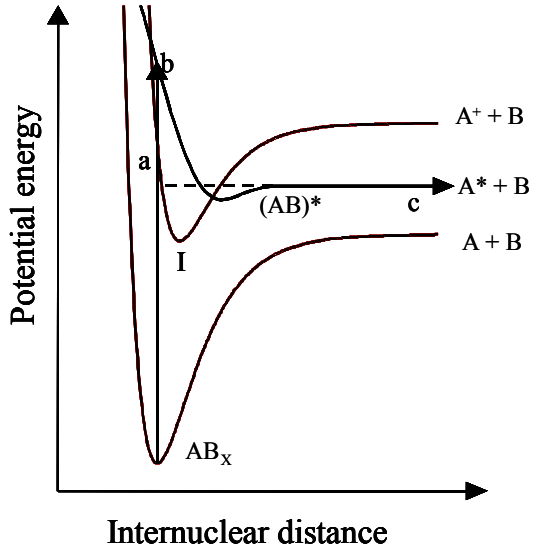

Fig. 3. Potential curves corresponding to neutral dissociation through a superexcited state (AB)*.

Note that the whole picture works for both attractive (AB)* states (as in Fig. 3) or repulsive (AB)* states as is further discussed in chapter 4 and papers I and II, as long as the dissociation limit is the same for both types of states. Therefore, from the explanation above it follows that by detecting the presence of the fragments A* and/or B, the dynamical path responsible for the production of these fragments can be followed. In papers I and II, the detection of the fragments is achieved by measuring the fluorescence produced by the excited atomic fragment A*, when it de-excites to a lower energy state by emitting photons, as schematized in Fig. 4. From the detected fluorescence, we can identify the states of the fragments produced. Hence, the energy level of the dissociation limit of the activated fragmentation channel can be established. Therefore, one can study the existing molecular states in the region and establish correlations, using theoretical computations, which explain the molecular dissociation through the observed fragmentation channels [5,32].

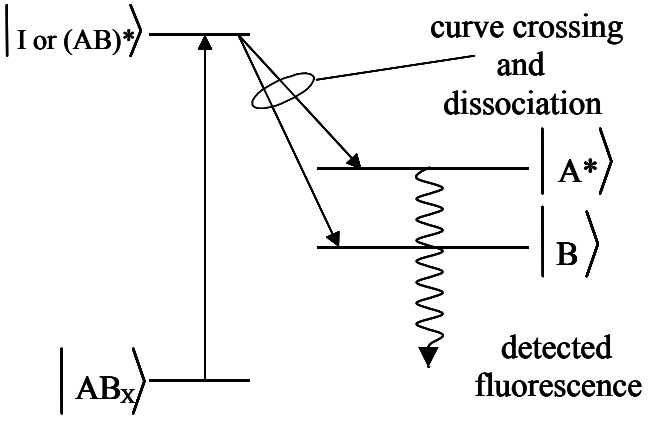

Fig. 4. Schematics of the neutral dissociation process studied in papers I and II. The atomic fragment A* is produced in an excited state which de-excites by emitting photons and the atomic fragment B is produced in its ground state and therefore, it does not fluoresce.

To interpret the non Franck-Condon effects and neutral dissociation observed in papers I to IV calculations are required providing information about candidate states which can be the origin for the observed spectra. The studies included in the thesis about neutral dissociation and non Franck-Condon effects have been analyzed by comparing the experimental results with many-body perturbation computations [33,34,35,36]. In section 2.5 the calculation method used and the nature of the molecular states involved in the studies presented in papers I to IV are discussed.

2.3 Dissociation after outer orbital ionization

When the photon energy absorbed is high enough to excite valence electrons to mainly Rydberg and continuum states there is a competition between autoionization and dissociation. If the excitation energy is high enough the ejection of the valence electron leads to an ion that is often predissociated by curve crossing with repulsive dissociative states or directly dissociated if enough excitation energy is transferred to vibrational energy of the nuclei [24]. A summary of the main processes in photoionization and photodissociation of molecules is schematized in Fig. 5 [37]. As the absorbed energy is larger than the Ionization Potential (I.P.) the molecule may be ionized and/or dissociated either via direct process or via doorway state (AB)*. For energies in the vicinity of the I.P. the latter process is the dominant and gives rise to ionic species (AB^+, $A^{\pm}$, $B^{\pm}$) or fluorescence from the excited ions or neutral alike. The $(AB)^+$ ion can be formed in this energy region via autoionization of the (AB)* state while the atomic ions can be formed in predissociation either into $A^+ + B^*$ or into ion pairs $A^+ + B^-$. However, autoionization of the excited fragments has also been observed for excitation energies around the I.P. [38]. The excited fragments might also fluoresce, as indicated in Fig. 5.

Nevertheless, autoionization occurring on a timescale of 10^{-12} to 10^{-15} seconds is together with predissociation the most important decay processes from neutral molecular excited states. For this reason, these neutral molecular excited states are rarely observed in photoemission spectroscopy [39].

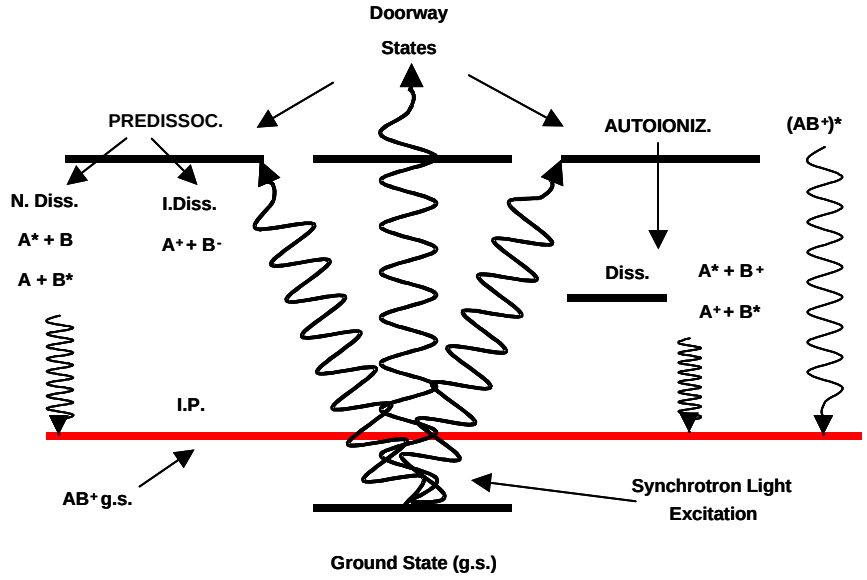

Fig. 5. Main processes in photoionization and photodissociation of molecules above I.P. schematized for a diatomic for simplicity. Neutral dissociation as well as dissociative ionization are included [37].

In papers V to VIII we study the dissociation after inner and outer valence ionization of CD_4 and SF_6 molecules (and after core excitation for the CD_4 molecule) by means of an energy resolved electron ion coincidence technique (discussed in detail in chapter 3). The excitation energies used in the valence studies are well above the I.P. (70 eV for CD_4 and 100 eV for SF_6) but below the core level excitation in both molecules, as exemplified in Fig. 6 for the SF_6 molecule [40]. The selective ionization of the different outer and inner valence orbitals in both molecules yields completely different mass spectra. The spectra reveal state dependent dissociation following distinct electronic states of the molecule. This dependence reflects the bonding properties of the potential surfaces involved in the studied processes. In case of the CD_4 studies the results are strongly influenced by the Jahn-Teller effect that distorts the CD_4^+ ground state after $1t_2$ valence electron ionization. Therefore, this effect is discussed in the following section. A summary of the results obtained is presented in chapter 4.

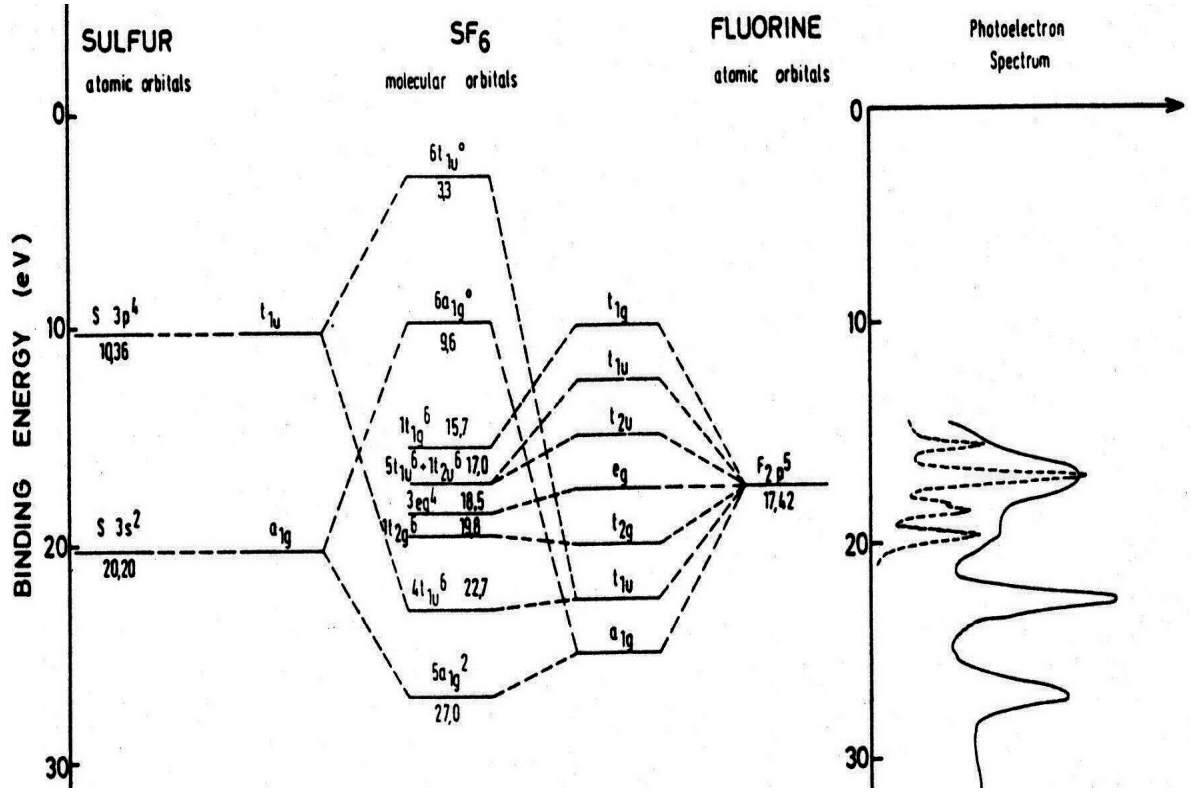

Fig. 6. Energy level diagram for the relevant SF_6 orbitals studied during the experiments presented in paper VII of this thesis. The orbitals studied are $(1t_{1g}+[5t_{1u}1t_{2u}])$, $(3e_g+1t_{2g})$, $4t_{1u}$ and $5a_{1g}$.

2.3.1 Jahn-Teller effect

In a degenerate electronic state there are several sub-levels (splitting) of each vibrational level if degenerate vibrational modes are excited. The excitation of degenerated vibrational modes yields as many component levels as many vibronic species exist in the particular vibrational level excited [41]. To evaluate the magnitude of the split components, Jahn and Teller considered the splitting of the potential function for non-totally symmetric displacements of the nuclei. They found that there is always at least one non-totally symmetric normal coordinate for which the splitting of the potential function is such that instead of two coinciding minima, there are two separate minima at nonzero values of the particular normal coordinate [42]. This is schematically shown in Fig. 7. The strong vibronic interaction distorts the degenerate molecular state and forces it to decay to a lower symmetry. This is the so-called Jahn-Teller effect.

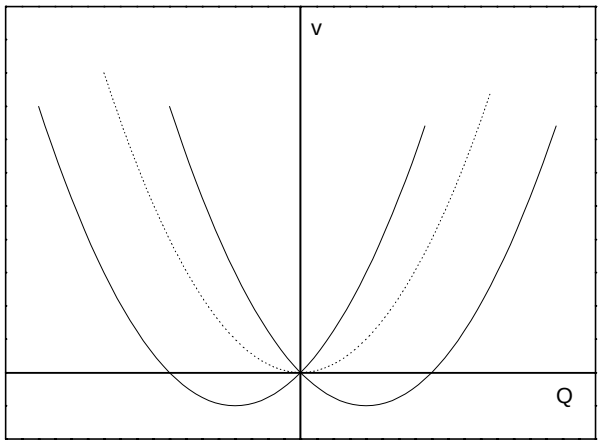

Fig. 7. Potential function projection of a non-linear molecule in a degenerate electronic state when the vibronic interaction is large. Q is a non-totally symmetric normal coordinate (usually degenerate) that gives rise to strong Jahn-Teller interaction. The zero vibronic interaction is shown as a dotted curve [41].

In the studies of methane (CH_4), which is a tetrahedral molecule with electronic configuration $(1a_1)^2(2a_1)^2(1t_2)^6$ as for deuteromethane (CD_4), it is shown that removing a $1t_2$ electron leaves a CH_4^+ ion in a $^2T_2$ state. This is a triply degenerate state strongly distorted by Jahn-Teller interactions. The Jahn-Teller distortion leaves the CH_4^+ ion in stable structures either in C_{2v} or C_{3v} symmetries [43]. This plays a crucial role in the dissociation of the CD_4^+ molecular ion after direct ionization of the outermost molecular orbital and also in the molecular relaxation by Auger decay as further discussed in chapter 4 and papers VI and VIII. For this reason a summary of the Auger decay processes is given in the next section.

2.4 Auger processes after core excitation

The creation of a core hole by core-level photoabsorption deposits a great amount of energy in the molecule. Therefore, fast electronic relaxation processes (in the order of 10^{-15} seconds) follow creating multiply ionized molecules in well-defined electronic states. These provide unambiguous starting conditions for the subsequent molecular dissociation processes [44]. The relaxation starts when an outer orbital electron fills the core hole formed. The initial state can be core-excited or core ionized, and can be regarded as an intermediate state between the initial and final states of the electronic excitation and subsequent relaxation process. The energy released by this process can be transferred to an ejected electron or emitted as a photon. When the electron carries the energy, the

process is know as Auger decay [45]. Depending upon whether the intermediate state is a core-to-valence/Rydberg excited state or a core-ionized state, one distinguishes between *resonant Auger* (populating two-hole one-electron (2h1e) or one-hole (1h) final states) and *(normal) Auger* decay (where two-hole (2h) final states are populated) [46].

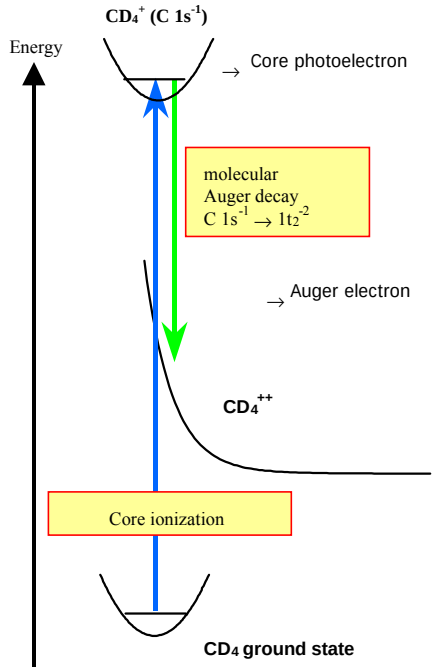

Fig. 8. Normal Auger decay scheme for the CD_4 molecule, from paper VI.

Normal Auger decay can be described as the ejection of the core electron to the continuum (using excitation energies higher than the threshold for core excitation) and the following Auger electron ejected when an outer electron fills the core hole. Hence, two electrons are promoted to continuum; the Auger electron and the core electron, giving rise to a doubly charged molecular ion. A scheme of the Auger process on the deuteromethane molecule is presented in Fig. 8. Resonant Auger decay refers to the Auger-like decay of core-excited molecules and covers several processes where the core electron promoted to the valence region remains as spectator or participates into the relaxation process. If the promoted core electron participates in the subsequent decay by filling the core hole the process is called *participator Auger decay* while if it stays in the valence region it is called *spectator Auger decay*. Hence, the participator final states (1h) are usually found at lower binding energies than the spectator final states (2h 1e) [46]. Fig. 9. presents a diagram for a two-step interpretation of such processes. For states where the core electron is promoted to Rydberg orbitals, which are far from the core hole, the spectator decay is a dominant process. For states where the core electron is promoted to a non-occupied valence orbital the participator decay process can also occur.

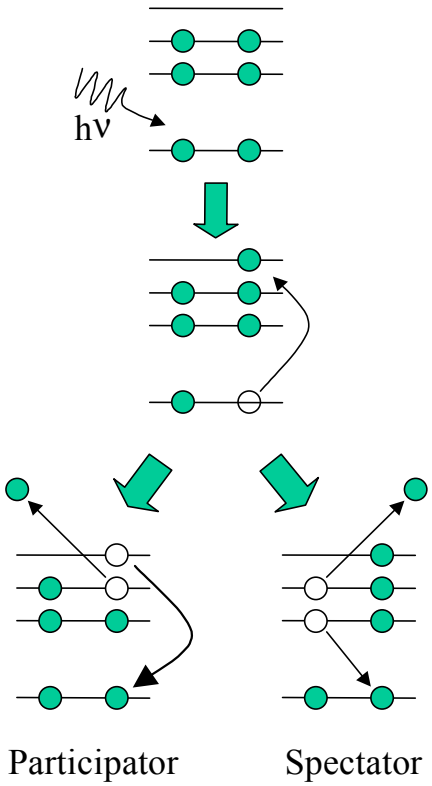

Fig. 9. The participator [(1h) final state, left] and spectator [(2h 1e) final state, right] models describing resonant Auger decay from core excited states.

Since the (1h) final state created by participator Auger decay (with a vacancy in a valence orbital) is the same as the final state reached by direct valence photoionization of the same valence orbital, participator Auger decay can be used as a probe to extract the effect of the nuclear motion in the core excited state [17]. This is the basis of the results obtained in the experiment described in paper VIII for the CD_4 molecule. A summary of the results is presented as well in chapter 4.

2.5 Computational methods

In papers I to IV *ab initio* calculations using many-body perturbation theory have been implemented to analyze the experimental data. Cross sections, branching ratios for photoionization, vertical excitation energies, transition moments and autoionizing rates of non Rydberg singly and doubly excited resonances have been computed. The full explanation of the method used is given in [33,34] and [35,36] respectively. Thus, just a brief summary of each part is given below.

2.5.1 Cross sections

The present method to compute cross sections for molecular photoionization is based on an integral equation that relates the real polarizability on the imaginary frequency axis to the photoionization cross section. Many-body perturbation theory with a complete perturbation expansion up to second order in the Coulomb interaction is used. This allows correlation effects to be comprehensibly included in the computations (together with interchannel coupling effects like the $2\sigma_u$ shape-resonance [47,48]). The computations obtain polarizabilities for imaginary frequencies from which the cross sections are calculated. The polarizabilities are obtained by inverting an integral equation using the analytic continuation method [33].

Summarizing, the dynamic polarizability $\alpha(\omega)$ represents the linear response of a molecule to an external electric field and can be formulated as

$$\mathbf{p} = \alpha(\omega)\cdot\mathbf{F} \tag{10}$$

where **p** is the electric dipole moment and **F** is the applied external field. Assuming a known form of the external field **F** and its orientation along the space fixed axis z, the corresponding time dependent external perturbative potential can be calculated. Hence, $\alpha(\omega)$ can be expressed in terms of the eigenvalues E_k and eigenstates $|\Psi_k\rangle$ of the zero field Hamiltonian. Consequently, the mean value of the electric dipole moment $\langle p\rangle$ and thus, the polarizability $\alpha(\omega)$ can be expressed in terms of the interaction between the external field and the zero field eigenstates $|\Psi_k\rangle$ mentioned above, using time dependent many-body expansion [33] as presented in eq. (11) where $|\Psi_0\rangle$ and $|\Psi_1^{\pm}\rangle$ are the components of the first order, time dependent wave function of the ground state $|\Psi^{(1)}(t)\rangle$.

$$\alpha(\omega) = \frac{\left\langle \Psi_0 \left| -\sum_{i=1}^{N} z_i \right| \Psi_1^{+} \right\rangle + \left\langle \Psi_0 \left| -\sum_{i=1}^{N} z_i \right| \Psi_1^{-} \right\rangle}{\left\langle \Psi_0 \Psi_0 \right\rangle} \tag{11}$$

Besides, the linear response of a physical system to an external perturbation is also given by the generalized polarizability (or susceptibility) $\alpha(\omega)$ defined as [49]

$$\alpha(\omega) = \int_0^{\infty} \alpha(t) e^{i\omega t} dt \tag{12}$$

Hence, since ω may now be regarded as a complex variable $\omega \rightarrow \omega + i\mu$ because the properties of the $\alpha(w)$ function defined in eq. (12), and by using the Kramers-Kroning dispersion relations for the real ($\mathrm{Re}\alpha(\omega)$) and imaginary ($\mathrm{Im}\alpha(\omega)$) parts of $\alpha(\omega)$ provided by eq. (12) and taking the Cauchy principal value of the resulting integrals, we can write

$$\alpha(i\mu) = \frac{2}{\pi}\int_0^\infty \frac{\omega \cdot \mathrm{Im}\,\alpha(\omega)}{\mu^2 + \omega^2} dt \tag{13}$$

Since the cross section of photoionization is given by Im$\alpha(\omega)$ [33] through

$$\sigma(\omega) = \frac{4\pi}{c} \cdot \omega \cdot \mathrm{Im}\,\alpha(\omega) \tag{14}$$

Combining eqs. (13) and (14) we obtain the integral equation that permits, using this method, to derive the values of the cross sections.

$$\alpha(i\mu) = \frac{c}{2\pi^2}\int_0^\infty \frac{\sigma(\omega)}{\mu^2 + \omega^2} d\omega \tag{15}$$

This is a Fredholm integral equation. Therefore, from the computed many-body values of $\alpha(i\mu)$ provided by eq. (11) it is possible to invert this integral equation to obtain the photoionization cross section, using a standard method, which is described in detail in [33]. Papers III and IV present partial cross sections or branching ratios which are computed for a series of internuclear separations around the initial state equilibrium internuclear separation. The necessary vibrational wave functions are obtained from known RKR ground state potential curves [50,51].

2.5.2 Non Rydberg excited states

The fragmentation or ionization dynamics of valence excited molecules can be studied using theoretical computations of existing molecular states in the region. These computations provide correlations between the experimental features and adequate candidate states. In papers I to IV, two types of autoionizing states appear as candidates to induce the observed effects: series of Rydberg states and non Rydberg singly and doubly excited states. The Rydberg states converging to the well known ionic states (Rydberg series) of the N_2 and O_2 molecules referred to in papers I to IV are well described in the literature [32,50,51,52,53] and therefore, they are not further discussed here since no computations have been required to identify them. Conversely, Non Rydberg Doubly Excited Resonances (NRDERs), although theoretically predicted long time ago [5], have remained experimentally unobserved until recently the first experimental evidence appeared [4]. However, detailed calculations of the excitation energies, transition dipole moments (oscillators strengths) and autoionization rates of the considered excited states (states lying usually well above the ionization threshold and therefore, decaying through autoionization) are required to positively identify the experimental features as NRDERs. Again, the method used for such calculation is many-body perturbation theory for general model spaces (quasidegenerate theory) [36]. This method has already been described in detail somewhere else [35,36]. Thus, here a brief summary is just included.

The main idea of the model used is to replace the complete exact stationary Schrödinger equation, $H \Psi_k = E_k \Psi_k$, (where $H = H_0 + V$ and $H_0 \Lambda_k = E_k^{(0)} \Lambda_k$) by a simpler effective one

$$H_{eff} \Psi^0_k = E_k \Psi^0_k \tag{16}$$

defined through the help of the following projection operators

$$P = \sum_{i \in P} |\Lambda_i\rangle\langle\Lambda_i| \qquad \text{and} \qquad Q = 1 - P \tag{17}$$

which acts as follows

$$P \Psi_k = \Psi^0_k \tag{18}$$

and the operator Ω which acts as reverse of P

$$\Psi_k = \Omega \Psi^0_k \tag{19}$$

Thus, the effective Hamiltonian is defined as

$$H_{eff} = P H \Omega P \tag{20}$$

which, after a lengthy derivation [36] leads to a workable perturbation expression for H_{eff} given as

$$H_{eff} = PH_0^S P + P(V - V_l)P + \sum_{i \in P} PV \frac{1}{E_i^{(0)} - H_0} \times QV|\Lambda_i\rangle\langle\Lambda_i| + \ldots \tag{21}$$

The exact energies of the system are obtained from eq. (21) by diagonalizing the resulting finite effective Hamiltonian matrix with elements

$$W_{kl} = \langle\Lambda_k|H_{eff}|\Lambda_l\rangle = W_{kl}^{(0)} + W_{kl}^{(1)} + W_{kl}^{(2)} \ldots \quad k,l \in P. \tag{22}$$

The transition moments are calculated in the following manner. Assuming that D_μ is a component of the electric dipole operator, using eq. (19) we can write

$$\langle\Psi_k|D_\mu|\Psi_l\rangle = \langle\Psi_k^0|\Omega^\dagger D_\mu \Omega|\Psi_l^0\rangle \tag{23}$$

The eigenstates of H_{eff} are linear combinations of members of the model space P, so

$$|\Psi_k^0\rangle = \sum_{i \in P} C_{ki}|\Lambda_i\rangle \tag{24}$$

where the coefficients C_{ki} are obtained by diagonalizing the matrix W_{kl} of eq. (22).

Thus the matrix elements of the effective transition moment operator within the model space $\Omega^\dagger D\mu\, \Omega$ are worked out from

$$\langle\Psi_k|D_\mu|\Psi_l\rangle = \sum_{i,j \in P} C_{kj}^* C_{li} \langle\Lambda_j|\Omega^\dagger D_\mu \Omega|\Lambda_i\rangle \tag{25}$$

in the same way as those of the effective Hamiltonian provided in eq. (22), up to a second order approximation.

The energy of a highly excited molecular state is generally above the ionization threshold of the molecules. Therefore, it usually decays via autoionization. Thus, the autoionization rates are calculated as follows

$$\left|\Psi(t)\right|^2 = e^{-\Gamma\frac{t}{\hbar}} \tag{26}$$

where Γ is the rate of autoionization. The lifetime of the state is thus $\tau = \hbar/\Gamma$. And the nonstationary character of the autoionizing states, leads to complex energies

$$z_0 = E - i\Gamma/2 \tag{27}$$

Thus, the autoionization rate is obtained from the small imaginary part of the complex energy. This imaginary part of the energy appears in the energy term $W_{kl}^{(2)}$ of eq. (22) after the derivation presented in [36]. In the papers I to IV presented in this thesis, the perturbation expansion is carried out to second order. The model space P used comprises 200-300 states of different symmetries and multiplicities. This allows for interactions between a large number of the most important configurations to be included. All the calculations of the vertical excitation energies, transition moments from the ground state and lifetimes are carried out at the ground state equilibrium internuclear distance for each studied molecule.

2.5.3 Dalton quantum chemistry program

In paper VI quantum chemistry calculations of the molecular structure and relaxation dynamics of the core ionized deuteromethane have been implemented to interpret the experimental data. The effort has been focused on the understanding of the dissociation of the doubly ionized molecule CH_4^{2+} (CD_4^{2+}) created by the electronic Auger decay. The energies and geometries used in the computations for the CH_4 molecule and its fragments have been obtained using multiconfiguration self-consistent-field (MCSCF) approach in the complete-active-space optimization employing the cc-pVDZ basis [54] set (except for the core ionized molecule). The calculations have been performed using the DALTON quantum chemistry code [55]. The code is a powerful quantum chemistry program for the calculation of molecular properties with SCF, MP2, MCSCF or CC wave functions. The strengths of the program are among others the areas of molecular potential energy surfaces, both for static and dynamical investigations. The latter aspect has been the one mainly employed in the study presented in paper VI. The program code, its characteristics and its full description are available at the web address: http://www.kjemi.uio.no/software/dalton/dalton.html. However, the flow diagram of the ***dynamic walk*** calculations implemented on the CD_4 molecule and discussed in paper VI is presented in Fig. 10 below.

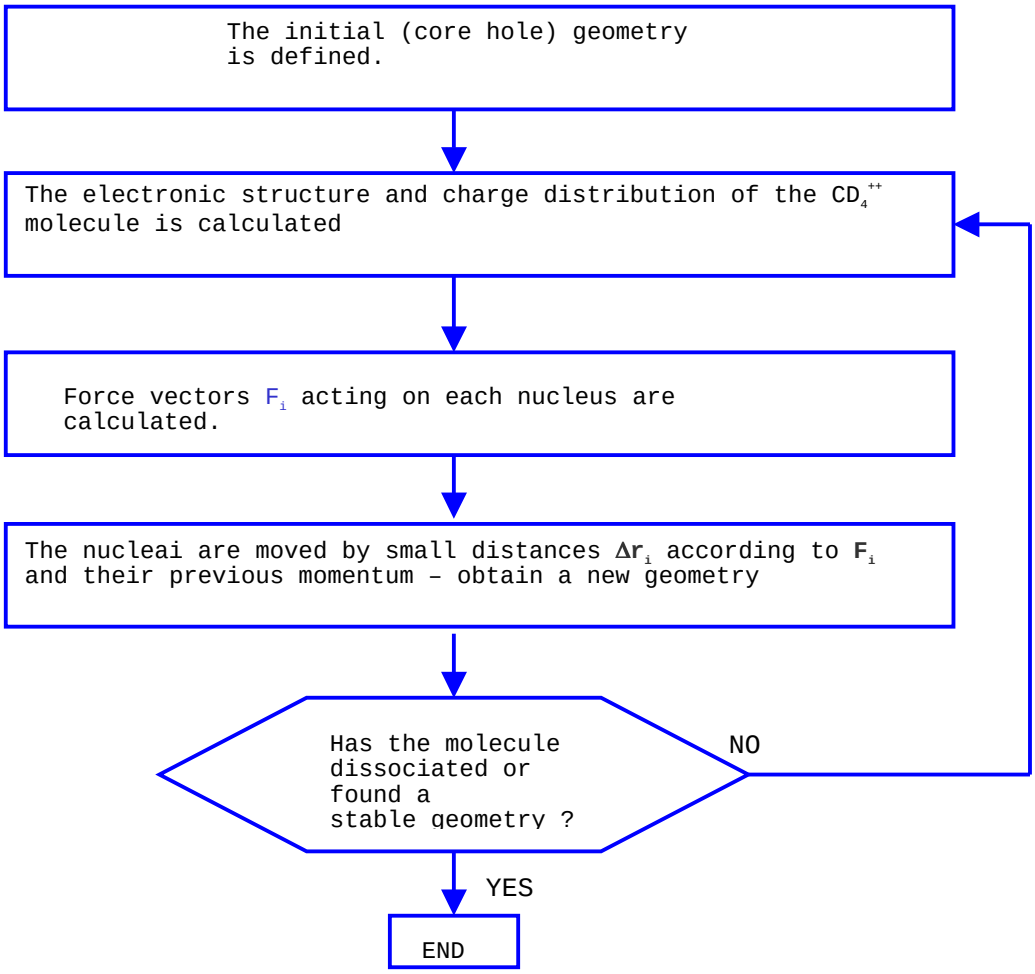

Fig. 10. Flow diagram of the dynamic walk computations implemented to obtain the molecular energies of the neutral and ionic CD_4 and its fragments by *ab initio* Hartree-Fock configuration interaction and multiconfiguration self-consistent field methods, using the program DALTON and the cc-pVDZ basis set [paper VI].

Chapter 3

Experimental method

The main objective of this thesis is to present the results obtained after four and a half years of experimental research. Therefore, it is necessary to present and comprehensibly describe the tools chosen to perform the studies included here. Below follows a brief summary of the light source used to generate the required excitation photons, MAX synchrotron radiation source. Next follows the different arrangements employed to deliver suitable synchrotron radiation frequencies depending on the experiments to be performed, MAX I beam line 52 and MAX II beam line I411. Then, a description of the experimental detection techniques used during the experimental beam times follows; dispersed fluorescence, photoelectron spectroscopy and energy resolved electron ion coincidences. Finally, the data analysis methods utilized to obtain the relevant physical information from the raw measured data are presented.

3.1 Synchrotron light

The MAX synchrotron radiation source in Lund, Sweden, presented in Fig. 11 provides the photons required to perform our experiments. MAX is a Swedish National Laboratory supporting three distinct areas of research: accelerator physics, research based on the use of synchrotron radiation and nuclear physics research using energetic electrons.

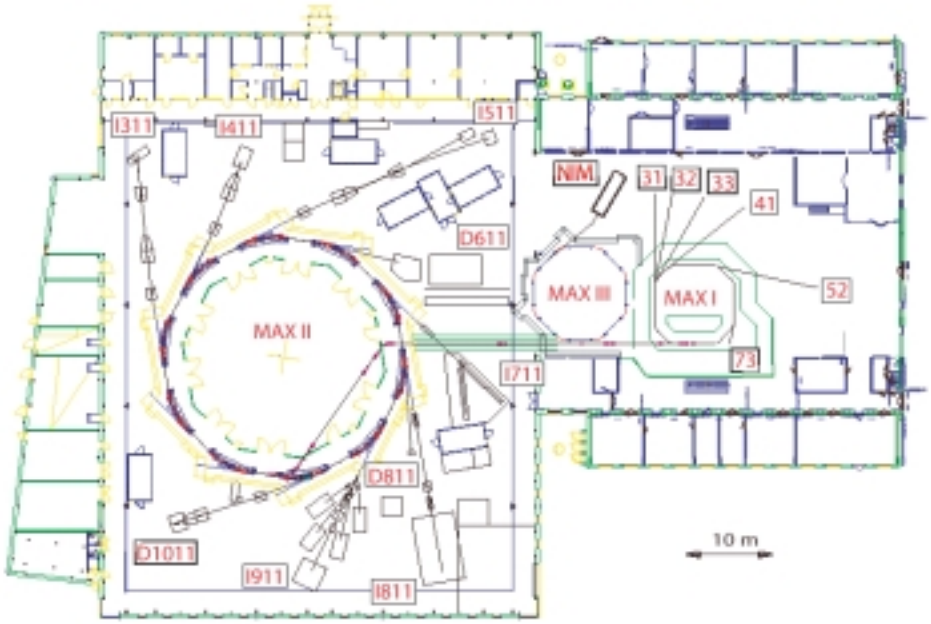

Fig. 11. Schematic of the MAX LAB synchrotron radiation source, in Lund. Three rings are currently present although only MAX I and MAX II are operational. The labels I411, 52, etc indicate the different beam lines [MAX LAB web site].

The facility consists of three different storage rings; one under construction (MAX III), which will operate at 700 MeV providing a source in the UV range, and two currently operative ones (MAX I and MAX II). MAX I is a 550 MeV electron storage ring in operation since the mid eighties. It is injected from a racetrack microtron operating at energies up to 100 MeV. MAX I has several operating modes: multibunch, single bunch and pulse stretcher for nuclear physics. MAX II is a 1.5 GeV third generation electron storage ring for synchrotron radiation. Table I shows the main storage ring parameters of MAX I and MAX II.

	MAX I	MAX II
Electron energy	550 MeV	1.5 GeV
Circumference	32.4 m	90 m
Current	250 mA	250 mA
RF	500 MHz	500 MHz
Bunch length	80 ps	20 ps
Beam lifetime	4 h	> 10 h
Number of straight sections	4	10

Table I. Main technical data of MAX I and MAX II storage rings [56].

3.1.1 Synchrotron light generation

The name *synchrotron light* comes after the type of machine in which this light was first observed, a synchrotron [57]. This machine is an electron storage cavity shaped as a closed ring, which inside is kept at ultra high vacuum (approximately 10^{-10} mbar). Inside the cavity are confined electrons traveling at speeds higher than 99.99% the speed of light, c = $3x10^5$ km/s. These electrons are forced by magnetic fields to bend at some points to follow the circular shape of the ring. At these bending points, the electrons emit radiation; i.e. light, in the forward direction. This light emission comes as a result of the force, which is acting on them when they are bent by an applied magnetic field. A much more detailed and advanced description of the synchrotron radiation and synchrotron facilities is widely available in the literature [57,58]. A summary of the different light generation within a synchrotron facility depending on the bending device used follows below, before describing in more detail the beam lines used for the experiments presented on this thesis.

An accelerated charged particle, as an electron in a synchrotron ring, emits light. Thus, depending on the device used to bend their trajectories synchrotron light with different properties is produced. The first and simplest devices generating synchrotron light are Bending Magnets (BM). They are non-straight paths of the storage ring where the electrons are deflected by dipole magnets. The radiation is emitted at the bending point in the forward direction. This light is highly polarized with the electric field vector **E** of the emitted radiation confined to the orbital plane and in the direction of the instantaneous acceleration; i.e. in the orbit's radial direction [58]. The second type of

devices used for synchrotron light generation is the so-called Insertion Devices (ID). These devices are straight sections inserted on the straight electron path of the ring. There are mainly two types of ID, *wigglers* and *undulators*. Both types consist of straight arrays of permanent magnets; one array is located above the electron trajectory (top) and the other below (bottom). The arrangement of the top and bottom arrays is such that the magnetic field is of alternating direction perpendicular to the electron path. Thus, the electrons wiggle their way through the correspondent ID. The main characteristics of each ID are the following:

Undulators: The light generation is based on constructive interferences. These constructive interferences take place when the period of the sinusoidal electron oscillation when passing through the undulator matches the wavelength of the emitted light [46]. Thus, the spectrum obtained from an undulator has sharp interference maxima spread over a wide energy range. The position of these maxima change by varying the strength of the magnetic field, which can be done in practice by changing the distance between the two arrays of permanent magnets (the so-called gap). The typical light properties of an undulator-based beam line are the following. The photon energy range is usually 50 to 1500 eV with typical energy resolution of $E/dE \approx 10^3$-10^4 and a flux of $\approx 10^{12}$-10^{13} photons/s. However, the exact values for the magnitudes listed above depend on the specifications of the optical elements mounted in the beam line.

Wigglers: These ID do not work with interference. The period of the magnetic field in a wiggler is smaller than the period of an undulator and the strength of the magnetic field is larger (some wigglers use superconductive magnets). Thus, wigglers usually generate photons with energy above 1500 eV. As with undulators the typical energy resolution is $E/dE \approx 10^3$-10^4 and the flux is $\approx 10^{12}$-10^{13} photons/s depending on the optical elements mounted in the beam line.

Although the light generated in the BM and ID has the basic characteristics to be useful in experiments, it needs several optical components to be transmitted to the experimental region with the proper focusing and spot size conditions and it needs a device which provides the user with the freedom to tune the light to a desired wavelength. These essential elements are external to the electron storage ring and are situated in what is usually referred as a beam line. The elements of a beam line determine the type of experiments that can be implemented. In the next sections the beam lines used for the experiments presented in this thesis are described.

3.1.2 MAX I beam line 52

MAX I beam line 52 (BL 52) source is a bending magnet. A summary of the main technical data about BL 52 is provided in Table II. The synchrotron light generated at the bending magnet hits a gold-coated spherical mirror 10 m away from the source point. This mirror focuses the radiation onto

the entrance slit of a 1 m normal incidence monochromator with a grating groove density of 1200 l/mm. Both the spherical mirror and the monochromator are kept under ultrahigh vacuum conditions (~10^{-10} mbar). The normal incidence monochromator (NIM) provides photons in the energy range of 5 to 35 eV. The monochromatic radiation is focused to the monochromator's exit slit, after which it enters a toroidal refocusing mirror chamber. There the light is refocused into the experimental chamber via a differential pumping stage. The light spot area at the focus point of the toroidal refocusing mirror is around 1 to 2 mm^2. The differential pumping stage permits measurements on gases as well as on solids [59], since in this stage the pressure is kept at 10^{-8} mbar by a cryopump. Fig. 12 presents a schematic of MAX I BL 52 used during the experiments discussed in this thesis.

MAX I Beam Line 52 Technical Data:	
Source:	Bending magnet.
Pre-focusing optics:	Spherical mirror.
Monochromator:	1 m NIM with 1200 l/mm grating.
Energy range:	5 - 35 eV.
Energy resolution E/dE:	~ 10^3.
Re-focusing optics:	Toroidal mirror.
Photon flux on sample:	~ 10^{10} ph/s.

Table II. Summary of the main technical data from MAX I BL 52 [60].

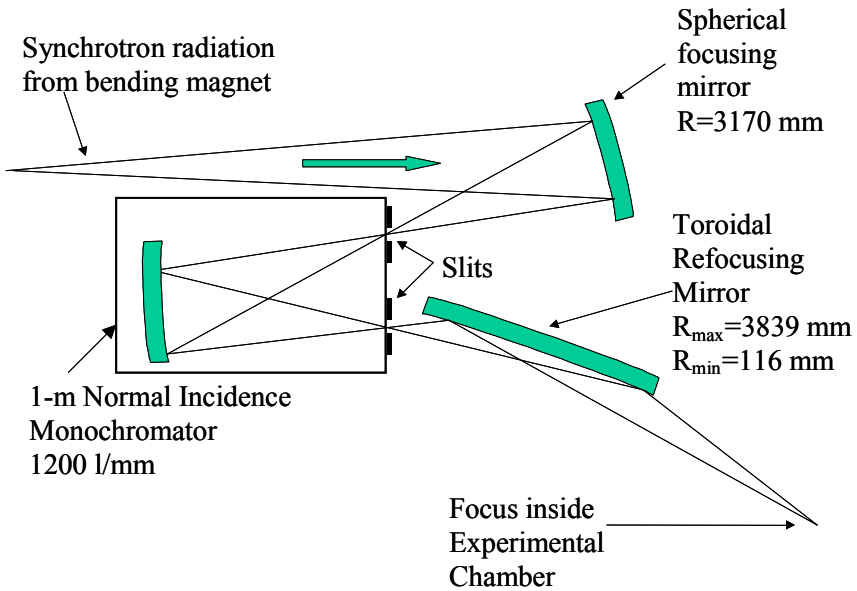

Fig.12. Schematic view of the MAX I BL 52 [60]. The different optical elements installed in the beam line are indicated.

The measured photon flux spectrum provided by BL 52 is presented in Fig. 13. This spectrum is measured using a Si-diode. The photon flux is peaked at 550 Å giving around 10^{10} photons/s with 200 μm slits at 100 mA ring current. Under these conditions the bandwidth of the generated radiation

varies between 60-120 meV in the 15 to 35 eV energy range. At wavelengths longer than 1000 Å there is a considerable contribution from higher order light [60]. This beam line has been used for all the experiments presented in papers I to IV.

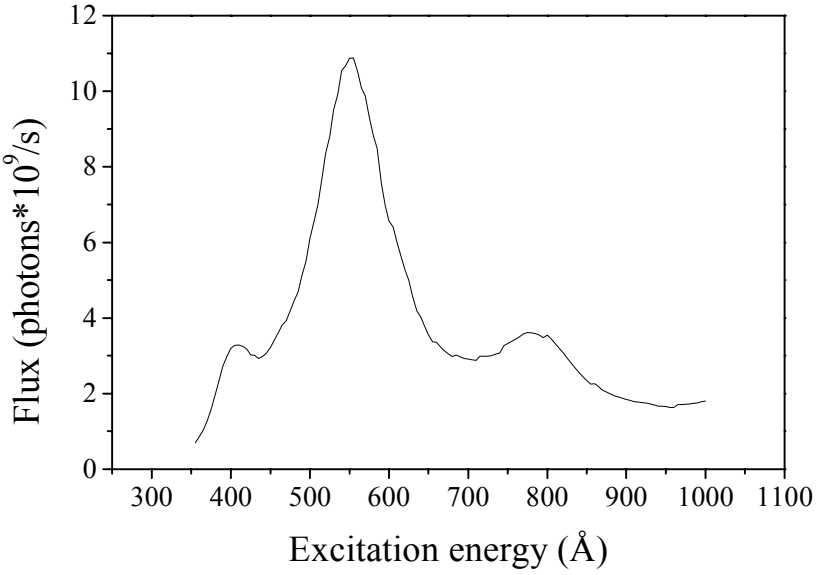

Fig 13. Photon flux from MAX I BL 52 from [60].

3.1.3 MAX II beam line I411

The soft X-ray beam line I411 [61] has been operational since January 1999. This beam line uses a high brilliance undulator photon source. The usable photon energy range in this beam line is from 50 to 1500 eV and a modified Zeiss SX-700 plane grating monochromator monochromatizes the radiation. The end station on the beam line is equipped with an angle resolving high resolution Scienta SES-200 hemispherical electron analyzer. Independently from the end station there is also a so called one-meter section, which is for users own experiments.

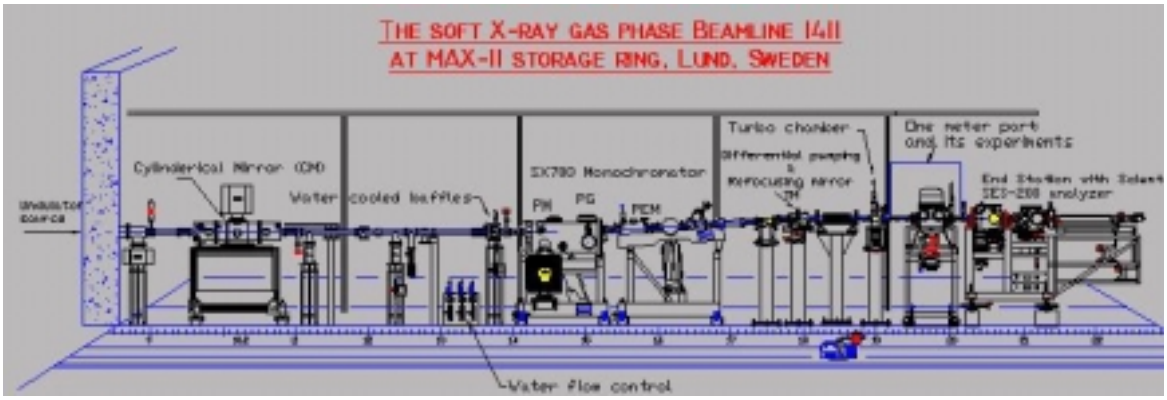

Fig 14. View of the MAX II beam line I411 with the installed elements [MAX LAB web site].

The experiments presented in papers V to VIII have been performed in this one-meter section. The experimental equipment was placed in it, having previously removed the existing one-meter vacuum pipe. However, in this beamline experiments can be done not only in gas phase but also in metal vapors, liquids and thin films using a wide range of spectroscopic techniques due to the features of the end station [62]. A view of the complete beamline is presented in Fig. 14. And the optical layout is schematized in Fig 15.

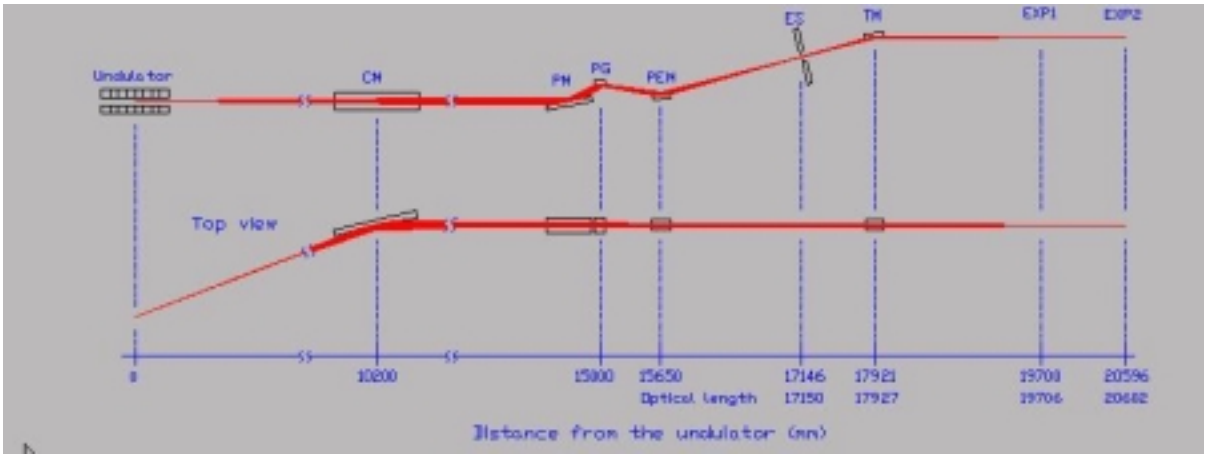

Fig 15. Optical layout MAX II beam line I411, EXP1 indicates the one-meter section [MAX LAB web site].

A summary of the main technical data about beam line I411 is provided in Table III below.

Beam Line I411 Technical Data:	
Source:	Undulator, period = 59 mm, 43 periods
Pre-focusing optics:	Horizontally focusing spherical mirror
Monochromator:	Modified SX-700 with 1220 l/mm grating and a plane-elliptical focusing mirror
Energy range:	50 - ~1500 eV
Energy resolution E/dE:	E/DE = 10^3 – 10^4
Re-focusing optics:	Toroidal mirror
Photon flux on sample:	10^{11} – 10^{13} ph/s

Table III. Summary of the main technical data from beam line I411.

The photon flux at the end station from beam line I411 is summarized in Fig. 16. Accordingly, having described how we can generate the light with the different characteristics necessary to perform the experiments, we proceed with the presentation of the experimental techniques used throughout the studies carried out.

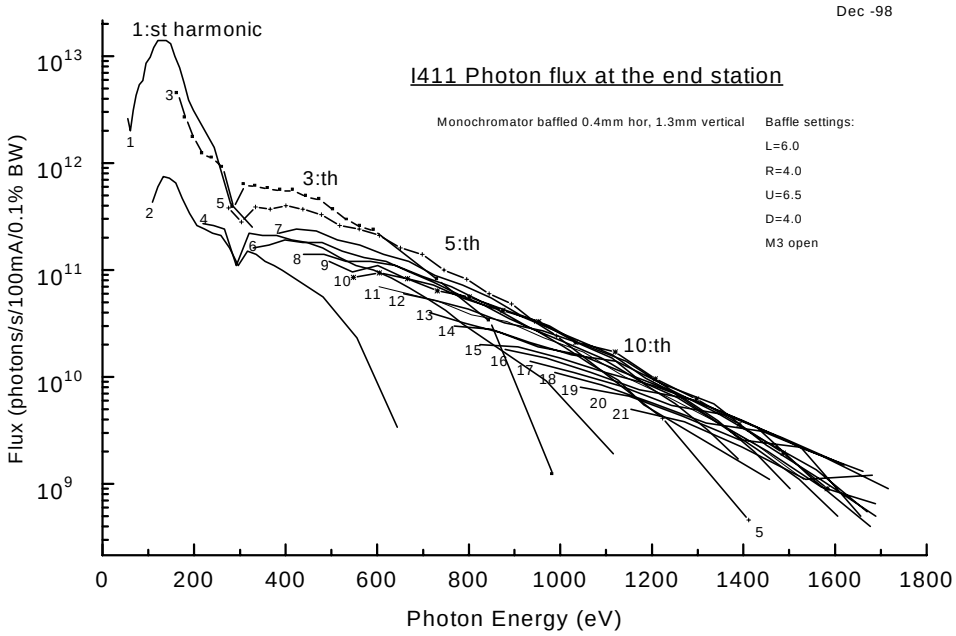

Fig 16. Summary of the photon flux from MAX II beam line I411 [MAX LAB web site].

3.2 Detection techniques

This section comprises the instrumentation and arrangements used to measure the quantities of interest i.e. which type of detectors and detection configurations are used. The data presented in the articles included in this thesis have been obtained using the following experimental techniques: Dispersed Fluorescence (DF), PhotoElectron Spectroscopy (PES) and Energy Resolved Electron Ion COincidences (EREICO), which are described in sections 3.2.1, 3.2.2 and 3.2.3 respectively.

3.2.1 Dispersed fluorescence

All the experiments performed using this detection technique were carried out at beam line 52. They are discussed in papers I and II and in chapter 4 of this thesis. Summarizing, after synchrotron photon absorption the molecules can break up into atomic fragments, some of them in excited states. These fragments can emit photons of different energies to get rid of the excess energy coming from the absorbed synchrotron photon at the beginning of the process. The emission of this light by the fragments created after the absorption on the synchrotron photon is called ***synchrotron radiation-induced fluorescence***. Since the fluorescence photons have different energies, it is necessary to select them by their energies to learn what has happened to the molecule after the photoabsorption process. This is called dispersed fluorescence technique.

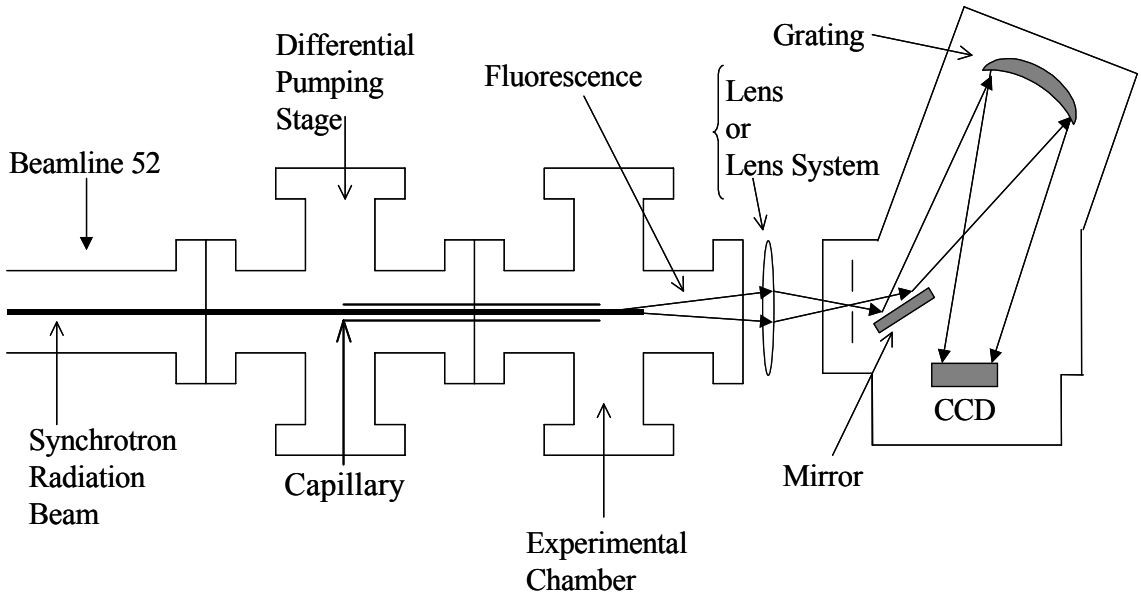

Fig. 17. Schematic view over the dispersed fluorescence experimental setup [60].

A schematic view of the dispersed fluorescence set-up used during the experiments is presented in Fig. 17. The dispersed fluorescence experiments are performed in the following manner. The synchrotron radiation from beam line 52 enters through a differential pumping chamber (10^{-7} mbar) into the experimental chamber, which is filled with the target gas (10^{-2} mbar) via a glass capillary of inner diameter 3 mm. The background pressures in the differential pumping stage chamber is kept in the 10^{-7} mbar range by several 60 l/s turbo-molecular pumps. The emitted fluorescence passes a glass window and is collected by a lens system and focused onto the entrance slit of Jobin Yvon spectrometer. This is a 46 cm spectrometer with 600 and 1200 grooves/mm gratings providing resolution of 1 Å in the 400-1000 nm range [63]. After passing the spectrometer the dispersed fluorescence reaches a CCD (charged coupled device)[(1)] position sensitive detector, which allows recording of an entire spectrum in one measurement [64]. This particular CCD system has a detector size 25 mm × 8 mm consisting of 1024 × 256 pixels and it allows high detection efficiency together with a low level of dark current[(2)] by using a liquid nitrogen cooling system [63]. A PC using commercial software displays the measured intensity as a function of wavelength and stores the obtained data.

[(1)]A CCD (charged coupled device) detector is a two-dimensional array of semiconducting pixels each capable of trapping the electrons originated in the semiconducting material by incoming photon, in a potential well. The acquired charge in each pixel after a certain acquisition time is readout by shifting the charge from one pixel to another until it reaches the output electronics. [(2)]Dark currents are leakage currents, which result in unwanted charge build-up in the pixels without any incident radiation. Dark currents have a strong thermal dependence.

3.2.2 Photoelectron spectroscopy

When the molecules of the studied gas absorb the incoming photons, they might break up into electrons, ions and neutral atoms. By measuring the velocities and directions in the space of the fragments produced after the absorption of the synchrotron photon, the process that creates them can be studied. In PES one measures precisely the velocities of the electrons. This has been performed during the experiments described in papers III and IV. A schematic view of the PES experimental station used is shown in Fig. 18. The photoelectron spectra of the studied gases are measured by letting the monochromatic photons into the experimental station. The experimental station consists of a vacuum chamber made of stainless steel, the vacuum equipment and the detection instruments. It is 1 m long (to be compatible with the requirements for beam line I411 in MAX II) and 1.25 m wide. It has more than 22 CF ports and more than 500 bolts! It has electro-polished inner surfaces to minimize the surface area, i.e. optimize the pumping speed. It can rotate 360 degrees around the synchrotron light axis with a rotation axis variation less than 50 μm to allow for angular resolved measurements. The vacuum chamber is kept under a constant background pressure below $5x10^{-6}$ mbar during the measurements by a couple of 250 l/s water-cooled turbo pumps, one evacuating the main chamber and the other pumping the spectrometer directly. A 300 l/s water-cooled turbo pump differentially pumps the used gas cell. There, the studied gas is confined with pressures 10-100 times above the chamber's ambient pressure.

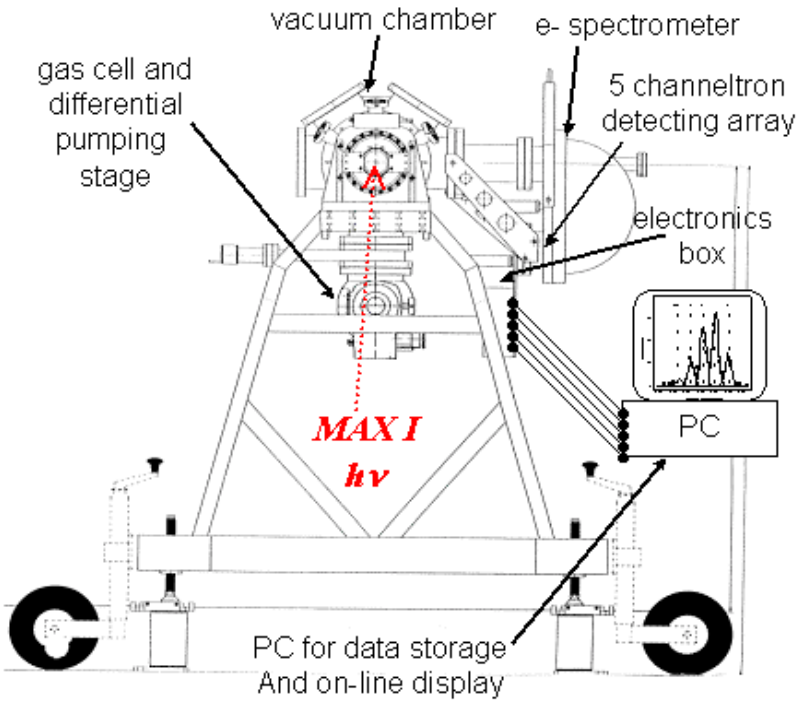

Fig. 18. Schematic view of the experimental station used during the PES measurements in MAX I BL 52.

The photoelectron spectra are acquired using a 125 mm mean radius electrostatic hemispherical electron deflection analyser [Omicron model EA125], presented in Fig. 19. It has variable entrance and exit rectangular slits, which can vary from 1x12 mm to 6x12 mm, or circular slits, from 1 mm to 6 mm diameter. The electron-collecting lens stack can be operated in low (x1), medium (x2) and high (x5) magnification modes. The EA is equipped with a five-channeltron array detector across the exit plane of the hemispherical analyser, placed along the dispersive direction. The best achievable electron kinetic energy resolution is about 6.5 meV for pass energy of 1 eV [65]. The electronics and data acquisition software can differ depending on the type of performed experiment. For the photoelectron spectra measurements implemented during the experiments involved in this thesis, a commercial electronics and data acquisition set is used. For electron-ion coincidence measurements, a home developed electronics and data acquisition arrangement can conveniently be installed, as discussed in the next section.

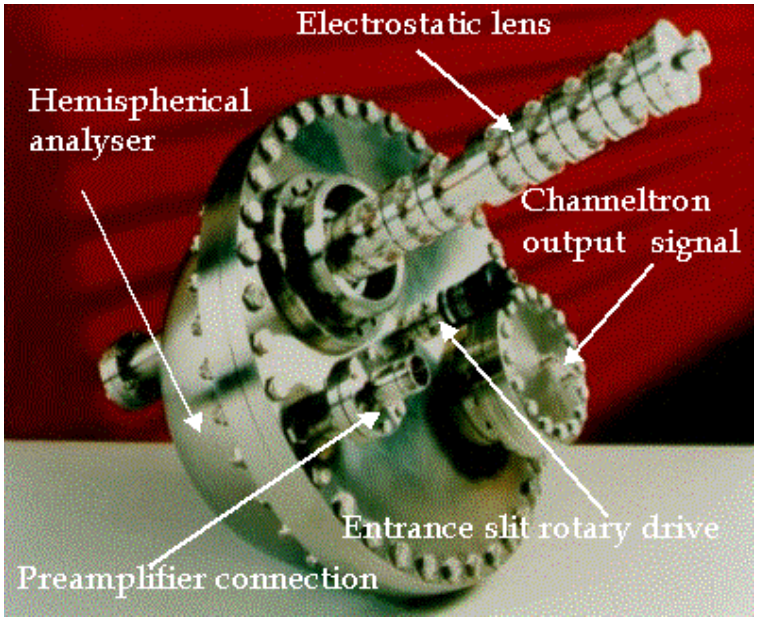

Fig. 19. The electron spectrometer used for the PES measurements.

During the experiments included in this thesis, the spectra have been measured with the electron spectrometer at the "magic" angle, 57.4 degrees with respect to the direction of the polarization of the synchrotron light, to remove the anisotropy of the emitted fragments [66].

3.2.3 Energy Resolved Electron Ion COincidence (EREICO)

This is the detection technique used during the experiments presented in papers V to VIII. The set up forms an electron-ion coincidence spectrometer schematically presented in Fig. 20 a). It comprises the 125-mm electrostatic hemispherical electron energy analyser described in the previous section, coupled with a modified Wiley-McLaren Time-Of-Flight (TOF) ion analyser. The TOF analyser is a home built, 119 mm free drift length instrument with the working parameters assuring the spatial focusing conditions [67]. The design parameters of this analyser are presented in Table IV.

IR radius (s) [mm]	First accelerating stage (d) [mm]	DT [mm]	Second accelerating stage (e) [mm]
1.5	3-3.5	119	2

Table IV. Summary of TOF spectrometer parameters. The distances s, d, DT and e are schematized in Fig. 20 b).

The scheme of the TOF analyser geometry is presented in Fig. 20 b). The TOF analyser is mounted on a goniometer allowing for its 0-90 degrees rotation with respect to the electron analyser entrance lens stack and perpendicularly to the photon beam. The axis of rotation is carefully aligned along the synchrotron radiation beam. A confined gas source, which is an integral part of the TOF spectrometer, provides a target pressure 10-100 times above the chamber pressure. During the measurements, the chamber pressure is kept constant below $6 \cdot 10^{-6}$ mbar. Again, the measurements are performed at the magic angle (54.7 degrees) with respect to the synchrotron light's polarization plane.

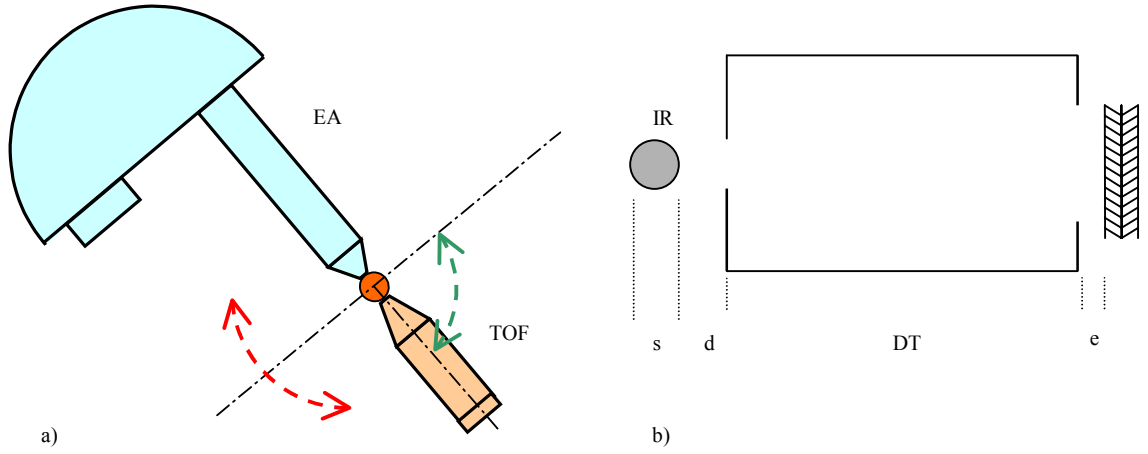

Fig 20. a) Electron-ion coincidence arrangement. b) Scheme of the geometrical TOF analyser parameters.

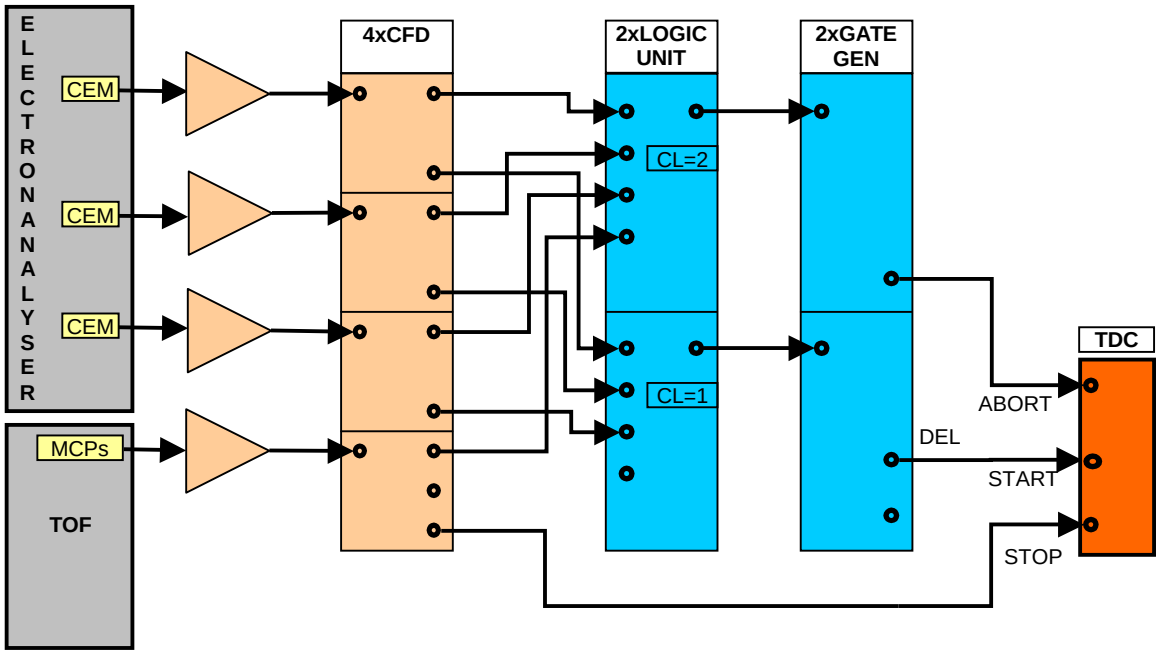

Fig. 21. Electronic and data acquisition arrangement used for EREICO measurements. The lower logic unit and gate generator panels represent the TOF measuring electronics. The upper logic unit and gate generator panels schematize the noise filter used (see text for details).

To perform the present EREICO measurements the following procedure is followed. Firstly, the electron spectra at the selected excitation energies are measured. The applied analyser settings (slits width, pass energy value, magnification mode) are chosen to achieve an optimal balance between electron detection efficiency and electron kinetic energy resolution needed. After tuning the synchrotron radiation to the desired photon energy the electron analyser parameters are set to detect electrons originating only from a chosen state. Thus, we ensure that only one particular electronic state is observed when registering the EREICO measurements. Next, the electron energy analyser commercial electronic and data acquisition system is replaced by a custom made set. The scheme of our electronic and data acquisition arrangement used for such EREICO measurements is presented in Fig. 21. Briefly, the signals from the EA channeltrons are collected and amplified by Ortec 120VT preamplifiers. Next, the signals are fed into Ortec CFD discriminators with a threshold set to discriminate the noise signals. From the discriminator outputs, the signals are fed into a logic unit with a level of coincidence 1, which ensures generation of an output pulse for each event at any of the inputs (e.g. the channeltrons). The output of the logic unit is connected to the START input of the Time to Digital Converter (TDC). The ion signal is generated from the micro channel plate detector of the TOF analyzer and amplified via an Ortec 120VT amplifier. The resulting signal is fed via the Ortec CFD to the STOP input of the TDC card. The TDC card is a PC extension card model 7886 by FAST Comtec. It is a 2 GHz real time multiscaler with time resolution of 500 ps per channel and maximum number of 2 million channels per spectrum. The card is installed in a PC with the appropriate software for data acquisition, storage and display. The electronic arrangement used avoids as well the loose of the measured spectra when electromagnetic noises existing in the environment of the laboratory

appear. The electromagnetic noise is characterized by the fact that if it affects the data acquisition electronics, it is picked up simultaneously in all detecting channels i.e. both in the electron and the ion detecting channels. Thus, by connecting all the detecting channels to a logic unit with a level of coincidence two, an output signal from the logic unit is generated every time any two detecting channels provide simultaneous inputs to the logic unit. This output signal is fed via a gate and delay generator to the ABORT input of the TDC card, which makes the card stop recording events for a prefixed period of time, as is represented by the upper logic unit and gate generator panels schematized in Fig. 21.

3.3 Data analysis techniques

The data analysis techniques are used to extract from the raw, measured data the information necessary to understand the studied physical process. This section presents the data analysis performed to the data obtained that leads to the results discussed in this thesis. The biggest concern of the data analysis processes described is to identify and extract from the raw data the instrumental- and noise-originated information before trying to understand and interpret it following a particular physical model as presented in sections 3.3.1 to 3.3.4.

3.3.1 Excitation functions

The conclusions on neutral dissociation presented in this thesis are deduced from the dispersed fluorescence data measured from synchrotron radiation excited O_2 and N_2 molecules. However, to reach such conclusions it is first necessary to study the variation of the intensity of a particular fluorescence emission line (I_a) as a function of the excitation energy (E_{exc}); i.e. it is necessary to obtain the so-called excitation functions. This, which might sound trivial provided the explanation of the DF experimental technique in section 3.2.1, is not so trivial if one considers all the processes involved in a single DF measurement, as the one presented in Fig. 22. For instance, by looking carefully at the spectrum, one can observe that the baseline of the spectrum slightly increases towards higher fluorescence wavelength.

This baseline mainly originates from the background photons recorded. Since the intensity of the different lines is only 10 to 50 counts above this baseline, one wants to completely remove whatever influence this baseline has on the intensity of the studied line. Since we are interested only in the peaks of the figure, (identified as emissions due to transitions between the two denoted excited states of N atoms) the baseline is removed by recording the same measurement without the N_2 gas in the chamber, the background spectrum, and subtracting it from the one measured with gas. The background spectrum has to be scaled by a constant to fit the baseline level of spectrum measured with gas, to compensate for the decrease in photon flux from the storage ring between consecutive acquisitions. Once these operations have been implemented the areas of the fluorescence lines under study are obtained using a software tool, which automatically fits a function to the peak and gives the area of the peak.

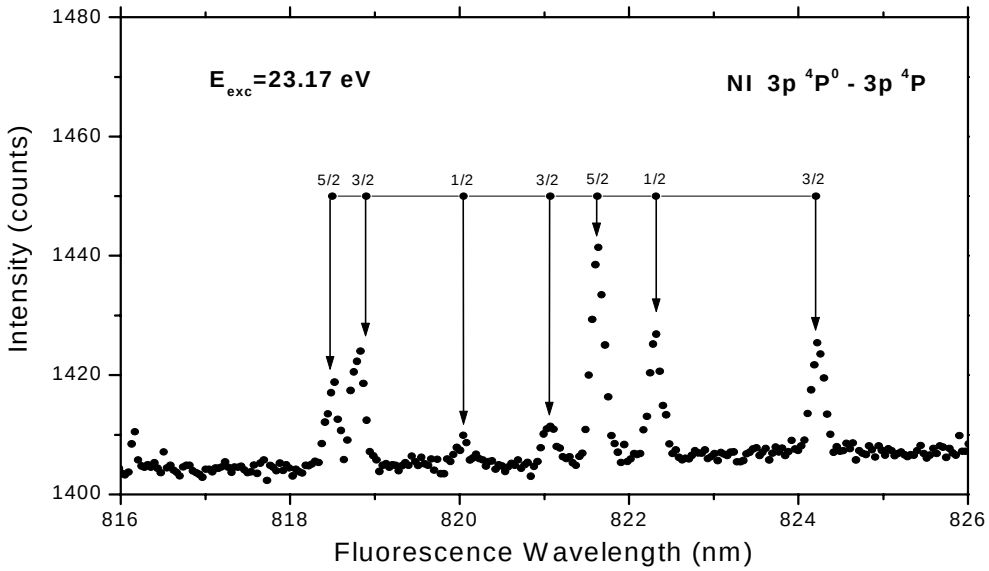

Fig. 22. Example of a DF raw, well resolved NI multiplet from synchrotron excited N atoms.

However, before using these areas to create the excitation functions, they have to be normalized against photon flux changes, since the photon flux differs with time and with photon energy, as shown in Fig. 13. This is necessary since the intensity of a fluorescence line is proportional to the number of excited atoms created in the particular state that fluoresces, and obviously this number of atoms in the excited state depends on the flux of incoming synchrotron photons. This normalization is implemented by measuring a reference molecular emission line (I_M) for which the relative emission cross section (σ_M) is well known from total fluorescence measurements. This procedure can be formulated as follows.

$$I_a^N(E_{exc}^i) = \frac{I_a(E_{exc}^i)}{I_M(E_{exc}^i)} \cdot \sigma_M(E_{exc}^i) \tag{28}$$

Thus, the area of the reference molecular emission line (I_M) divides the area of the fluorescence line under study (I_a). Then, the result is multiplied by the relative emission cross section value (σ_M) of the reference molecular line measured, for the excitation energy at which the spectrum was recorded. Hence, the normalized intensity of the fluorescence line under study (I_a^N) at a particular excitation energy (E^i_{exc}) is obtained. This value is free from errors originated by photon flux and gas pressure changes and background photons during the measurement. Thus, it can be used to learn about the variation of the studied fluorescence line throughout the excitation energy region studied. However, this value cannot be used to compare the relative populations of two different initial states giving rise to two different fluorescence lines because this value neither has been normalized against the quantum efficiency of the detector (Q_{eff}) nor has been corrected by the different transition rates or Einstein coefficients (A_{nl}) for each of the transitions giving rise to the fluorescence lines that are to be compared. These corrections are necessary because the detector has a different detection efficiency (quantum efficiency, Q_{eff}) for different detected light wavelengths (λ_{fl}) and because different transitions between two atomic levels are characterized by different transition rates, A_{nl}. Once these corrections have been made information about the number of atoms in the initial (upper) state can be obtained from the measured intensity of a fluorescence line as follows.

$$N_R^j(E_{exc}^i) = \frac{I_a^N(E_{exc}^i)}{A_{nl}(\lambda_{fl})} \times Q_{eff}(\lambda_{fl}) \tag{29}$$

Thus, N^j_R is the relative population of the state **j** corresponding to the fluorescence line (λ_{fl}) at the excitation energy E^i_{exc}**.** By applying eqs. (28) and (29) to each measured fluorescence line intensity corresponding to an atomic transition, the relative populations presented in paper I are obtained. There, the NI fluorescence lines corresponding to the transitions 3p $^4S^0$-3s ^4P, 3p $^4P^0$-3s ^4P, 3p $^4D^0$-3s ^4P and 3p $^2D^0$-3s ^2P ($\equiv I_a$) are measured and normalized by the N_2^+ B $^2\Sigma_u^+ - X\ ^2\Sigma_g^+$ (0;0), (0;1) and (0;2) molecular fluorescence lines ($\equiv I_M$). The (0;0) molecular fluorescence line is used to normalize the 3p $^4S^0$-3s ^4P, 3p $^4P^0$-3s ^4P atomic emission lines since it is recorded in the same spectra. The (0;2) molecular line is used to normalize the 3p $^4D^0$-3s ^4P and 3p $^2D^0$-3s ^2P atomic emission lines since they are recorded in the same spectra. And the (0;1) molecular line is used to normalize both sets of measurements between themselves, since the four atomic transitions cannot be recorded at the same

time in only one spectrum. The σ_M for the N_2^+ $B\ ^2\Sigma_u^+ - X\ ^2\Sigma_g^+$ (0;0), (0;1) and (0;2) molecular lines is known from previous measurements [68]. In paper II the excitation functions obtained are a slight variation of the ones provided by eq. (29). They are defined as formation ratios (ξ_{nl}), which provide the cross section for dissociation of the molecules of the target gas into a particular channel. They are obtained by applying the following equation.

$$\xi_{nl}^{j}(E_{exc}^{i}) = \frac{I_a^N(E_{exc}^{i})}{\tau \cdot A_{nl}(\lambda_{fl})} \times Q_{eff}(\lambda_{fl}) \tag{30}$$

where τ is the lifetime of the *nl* state. Thus, this is the ratio of molecules that dissociate to a particular excited atomic state **j** corresponding to the fluorescence line, λ_{fl} at particular excitation energy, E^i_{exc}. In paper II, the OI fluorescence lines corresponding to the atomic transitions 3p ^{5}P-3s ^{5}S^0, 3p ^{3}P-3s ^{3}S^0, 4d ^{3}D^0-3p ^{3}P, 5 to 7s ^{3}S^0-3p ^{3}P, 5s ^{5}S^0-3p ^{5}P and 4 to 5d ^{5}D^0-3p ^{5}P ($\equiv I_a$) are measured and normalized by the O_2^+ $b\ ^4\Sigma_g^- - a\ ^4\Pi_u$ molecular fluorescence lines ($\equiv I_M$). The σ_M for these molecular lines is known from previous measurements [53]. *"…estesuno…entonses…"* [69]

3.3.2 Branching ratios

The non Franck-Condon studies presented in papers III and IV are obtained by measuring photoelectron spectra of synchrotron excited O_2 and N_2 molecules, respectively. As explained in chapter 2, from the Franck-Condon principle follows that the ratio between two vibrational transitions of two different electronic states should be almost constant, independent on the excitation energy, as long as the transition occurs in a direct vertical way. Thus, as long as we detect a fingerprint of two different vibrational transitions between the same electronic states of a molecule, we can apply the branching ratio data analysis technique.

PES vibrational branching ratios. A typical PES spectrum of the O_2^+ system studied in paper III is presented in Fig. 23. The fitted Gaussians provide an area for each peak. These areas (A) are proportional to the population of the corresponding vibrational state and they are used to calculate the vibrational branching ratios presented in papers III and IV. These branching ratios, R, can be expressed as follows

$$R(E_{exc}^{i}) \propto \frac{A_{v=1-3}(E_{exc}^{i})}{A_{v=0}(E_{exc}^{i})} \tag{31}$$

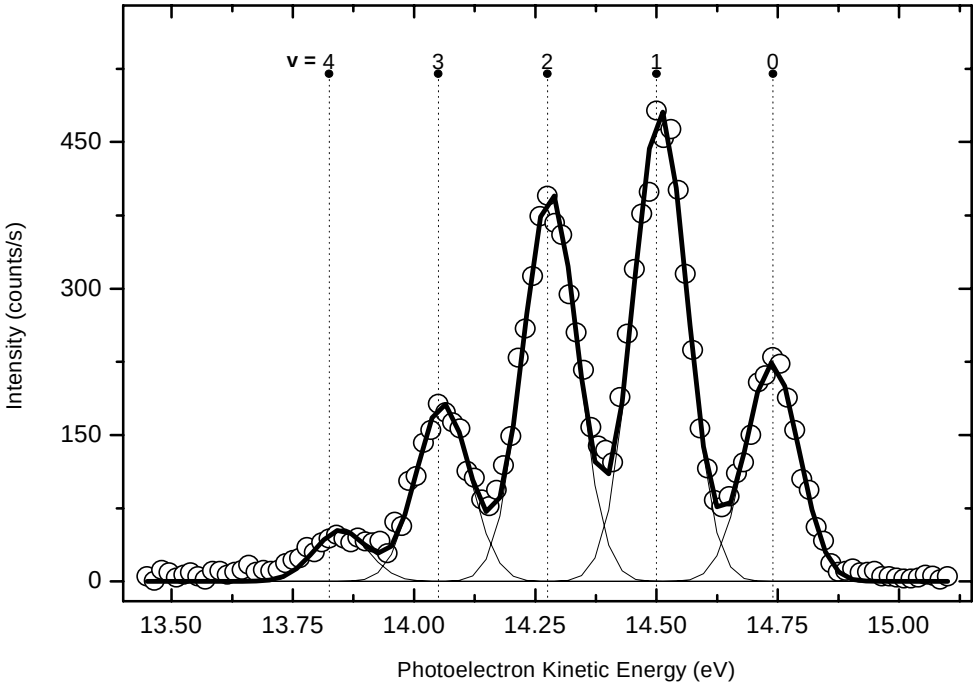

Fig. 23. Typical O_2^+ PES spectrum (o) acquired at excitation energy of 27 eV. The spectrum is deconvoluted using Gaussian profiles (thin full lines). The thick full line indicates the sum of all the fitted Gaussians.

Consequently, the branching ratio technique becomes a very sensible tool to probe the existence of autoionizing states through the observation of non Franck-Condon effects. The non Franck-Condon studies of synchrotron excited O_2 and N_2 molecules are summarized in chapter 5 and discussed in papers III and IV.

3.3.3 Time of flight peak simulating code

The basis of the EREICO technique used is the measurement of the ion TOF by detecting the ions in coincidence with energy resolved electrons. The electron analyser provides the start signal for the timing electronics and the signal from the multichannel plate detector mounted in the Wiley-McLaren TOF ion analyzer provides the stop, as indicated in Fig. 21. The TOF values measured by this type of analyzer depends on the mass (M) to charge (Q) ratio of the detected fragment [67]

$$T \propto \sqrt{\frac{M}{Q}} \tag{32}$$

Thus, different fragment masses can be identified from the TOF values obtained when measuring the mass spectra. The TOF is also proportional to the projection of the initial momentum of the ion in the direction of the analyzer axis [60,67]. Thus, it is possible to obtain information about the translational kinetic energy of the detected fragments and even total kinetic energy released in the dissociation process in two-body reactions by simulating the mass spectra peak shapes [60]. In all the experiments presented here the voltages applied across the interaction region (IR) for directing the ions into the TOF analyzer are relatively low. Therefore, the mass spectra peak shapes observed are strongly influenced by the kinetic energy of the ions. This is corroborated by the peak broadening and even splitting observed in the case of fast ions, originated by the delay in entering the analyzer between the ions moving initially away and those moving towards the analyzer, as in Fig. 24.

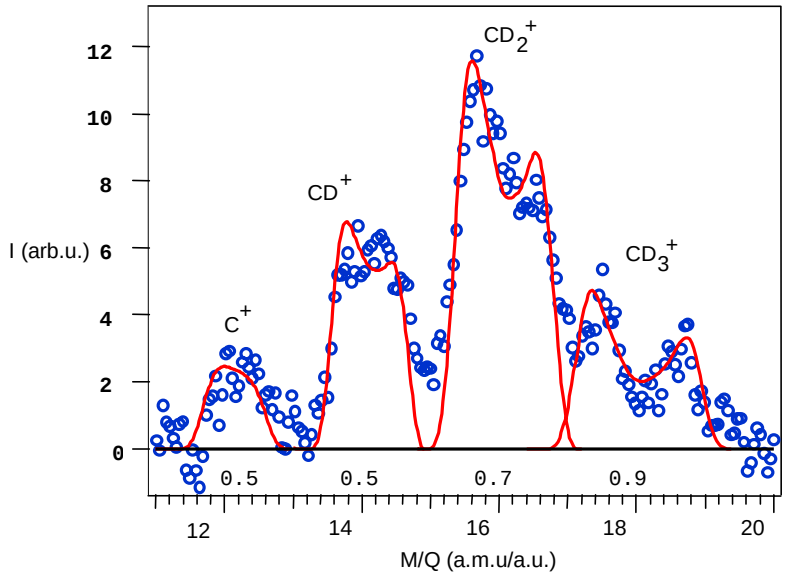

Fig. 24. A region of an EREICO spectrum acquired at excitation energy of 350 eV, from paper VI. The circles are the experimental spectrum and the lines the simulated peak shapes. Underneath each peak the calculated fragment's kinetic energy is given.

From the EREICO mass spectra measured throughout the experiments discussed in papers V to VIII, values for the kinetic energies of the observed fragments are obtained from the different time of flight mass spectra peak shapes using the derivation from [67] including the kinetic energy of the fragment. The values determined for the kinetic energy of the fragments and total kinetic energies released in the different reactions studied have been estimated through Monte Carlo simulations of candidate dissociation processes in each case, using the simulating code written by Ph.D. P. Winiarczyk and Prof. M. Stankiewicz in Borland Delphi programming language.

The simulating code tries different total kinetic energy released values until a best fit is obtained for each measured TOF peak. The code's computed TOF take into account the delay introduced by our data acquisition electronics, which is a value around hundreds of ns, the exact values depending on the characteristics of electronic components for each specific experiment (length of LEMO cables used, delay of electronic units, etc…). Besides, the electron TOF from its creation in the IR to its detection in the EA is also taken into account in the simulating code. The electron TOF in the EA depends on the pass energy of the EA and on the kinetic energy of the selected electrons. Thus, this can introduce different shifts from measurement to measurement with respect the expected TOF obtained by numerical simulations using the TOF equations from [67]. Therefore, this electron TOF is considered in the simulating code as follows. The electron mean kinetic energy (<*k.e.*>) is obtained as the average between the set kinetic energy for the electron analyzer ($k.e._{EA}$) and the set pass energy (E_p), as indicated in eq. (33).

$$\langle k.e. \rangle = \frac{k.e._{EA} + E_P}{2} \tag{33}$$

The electron TOF in the lens stack and in the hemisphere of the EA is calculated as follows. Firstly, it has to be stated that the length of the lens stack (L_l) is determined to be 0.45 m and the length of the 125 mm hemisphere is about 0.4 m. Secondly the kinetic energy of the electrons can be expressed as

$$k.e._{e^-} = \frac{1}{2}mv^2 = \frac{1}{2}m\left(\frac{L}{t}\right)^2 \tag{34}$$

Thus, the time of flight (t) of the given electron with kinetic energy $k.e._{e^-}$ in the length L is

$$t = \frac{L}{\sqrt{\frac{k.e._{e^-}[eV] \times 1.6 \cdot 10^{-19} \left[J/eV\right] \times 2}{m_{e^-}[kg]}}} \tag{35}$$

The code generates the simulated ions according to a given kinetic energy distribution and the ions are emitted isotropically. This energy distribution is then adjusted until the best fit to the measured TOF peak is obtained. The simulations also account for the finite size of the source volume and the photon beam, but since space focusing conditions are fulfilled, these factors have only a minor effect on the peak shape [60,67]. The code assigns also to the ions a certain Gaussian kinetic energy

spread centered at the given kinetic energy values. This spread can be viewed as due to the projection of the initial states wave function onto the potential energy surfaces of the final states involved. The simulating code has been the basis of Ph.D. P. Winiarczyk thesis and therefore it is fully described there [70].

3.3.4 Error calculation

The different excitation functions and branching ratio spectra presented in this thesis include the respective error bars associated to each experiment. These error bars have been calculated by applying error propagation theory [71]. In particular the calculation of the standard deviation (mean error) $\Delta\sigma$, for each of the experimental functions (excitation functions and branching ratios) described in the former sections can be written as follows:

$$\Delta\sigma_{F(x_i,\ldots,x_n)} = \sqrt{\sum_{i=1}^{n}\left(\frac{\partial F}{\partial x_i}\cdot\Delta x_i\right)^2} \tag{36}$$

Where $F(x_i,\ldots,x_n)$ is the experimental function used, x_i are the different variables of the function, which are experimentally measured, and Δx_i are the instrumental errors associated to the measurement of the variable x_i. Thus, the error bars associated to each experimental point of the spectra are calculated using eq. (36). However, the magnitude of the bars might be one to four times the value obtained from eq. (36). Table V presents the confidence intervals for each of these error bars magnitudes.

	$\Delta\sigma$	**2 x $\Delta\sigma$**	**3 x $\Delta\sigma$**	**4 x $\Delta\sigma$**
Confidence Interval (%)	70	95	99	99.9

Table V. Confidence intervals for the different error bars magnitudes [71].

Chapter 4

Results

A more complete description of the systems studied N_2, O_2, SF_6 and CD_4 molecules is necessary here so the obtained results can be better framed within the existing knowledge for each of them. Some molecular data of interest, relevant for the studies performed are given bellow. The neutral dissociation processes presented in papers I-II themselves are a modest surprise, since the energy of the photons used is well above the ionization limit of the two molecules studied, as presented in Table VI.

Molecule	Ionization potential (eV)	Neutral dissociation energy range (eV)	Photoionization energy range (eV)
N_2	15.58	20-30	20-34
O_2	12.07	15-25	19-34

Table VI. Ionization potentials [72] and synchrotron energy ranges scanned during the studies presented in this thesis.

Thus, some kind of interaction occurring in the excited states in which the molecule ends up just after absorbing the synchrotron photon makes the absorbed energy to be used to break the bond between nuclei and yield two neutral, atomic fragments instead of being used to ionize the molecule. Secondly, papers III and IV present non Franck-Condon effects in the photoionization channels studied, which implies that the molecules, after absorbing the photon, do not immediately eject an electron and reach an ionic state, but instead they reach different neutral excited states. From these neutral excited states the molecules eventually eject an electron (autoionize) and reach the corresponding final ionic state, but in a very different way if we compare with those molecules that absorbed the photon, ejected the electron and directly reached the same final ionic state. A reminder of the electron configurations of the N_2 and O_2 molecules is given in table VII. Tables VIII and IX provide the electron configurations and the energies necessary to liberate an electron from a particular orbital of these two molecules.

Molecule	Ground state term	Electron configuration
N_2	$^1\Sigma_g^+$	$1\sigma^2_g\ 1\sigma^2_u\ 2\sigma^2_g\ 2\sigma^2_u\ 1\pi^4_u\ 3\sigma^2_g$
O_2	$^3\Sigma_g^-$	$1\sigma^2_g\ 1\sigma^2_u\ 2\sigma^2_g\ 2\sigma^2_u\ 3\sigma^2_g\ 1\pi^4_u\ 1\pi^2_g$

Table VII. Electron configurations of the N_2 and O_2 molecules [72,73]

N_2	Electronic (Ionic) state	Electron configuration [50]	Vertical binding energy (eV) [72]
	$X\ ^2\Sigma_g^+$	$3\sigma^1_g$	15.58
	$A\ ^2\Pi_u$	$1\pi^3_u$	16.93
	$B\ ^2\Sigma_u^+$	$3\sigma^1_g\ 1\pi^3_u\ 1\pi^1_g$	18.75
	$C\ ^2\Sigma_u^+$	$3\sigma^1_g\ 1\pi^3_u\ 1\pi^1_g$	25.51
	$D\ ^2\Pi_{gi}$	$1\pi^2_u\ 1\pi^1_g$ (3)	26.00

Table VIII. The most relevant N_2 ionic states for the work presented in this thesis, their respective electronic configurations and vertical binding energies.

O_2	Electronic (Ionic) state	Electron configuration [51]	Vertical binding energy (eV) [73]
	$X\ ^2\Pi_g$	$1\pi^1_g$	12.31
	$A\ ^2\Pi_u$	$1\pi^3_u$	17.64
	$b\ ^4\Sigma_g^-$	$3\sigma^1_g$	18.17
	$B\ ^2\Sigma_g^-$	$3\sigma^1_g$	20.30
	$3\ ^2\Pi_u$	$1\pi^3_u$	23.90
	$c\ ^4\Sigma_u^-$	$2\sigma^1_u$	24.56

Table IX. As in Table VIII but for the O_2 ionic molecular states.

Recently, experimental and theoretical studies of the predissociation of the $2\sigma_u^{-1}$ ($c^4\Sigma_u^-$) $n\sigma_g$ $^3\Sigma_u^-$ Rydberg series in O_2, R(c) nsσ, [74] confirmed our results presented in paper III, where we assigned a strong non Franck-Condon feature around 21 eV in the branching ratio v=3/v=0 of the photoionization to the O_2^+ $X\ ^2\Pi_g$ state to autoionization of the v=0 and 1 levels of the R(c) series. There it was shown that the R(c) nsσ v=0 level mainly autoionizes while v=1 competes with predissociation. Moreover, electron spectroscopy studies of a new series converging to the $b\ ^4\Sigma_g^-$ state of O_2^+ in the 19 eV region [75] show that autoionization of higher vibrational levels of these series and NRDERs that couple to Rydberg states in this energy region need to be taken into account. These data are missing in our figure 4 of paper III. They would confirm our assignment of the strong non Franck-Condon feature observed from 19 eV to 22 eV and perhaps it would also contribute to explain the origin of the strong previously unobserved Franck-Condon breakdown up to 28 eV. In case of the N_2 molecule, high resolution photoelectron spectroscopy studies of the X and B ionic states [76] present non Franck-Condon effects in the X state, as already observed [4] whereas the B state does not show them in the energy region studied, as in paper IV.

For the coincidence experiments presented here, Table X below presents the electronic configurations of the SF_6 and CD_4 molecules.

Molecule	Ground state symmetry	Ground state electron configuration
SF_6	O_h	$1a_{1g}^2\ 2a_{1g}^2\ 1e_g^4\ 1t_{1u}^6\ 3a_{1g}^2\ 2t_{1u}^6\ 4a_{1g}^2\ 2e_g^4\ 3t_{1u}^6\ 5a_{1g}^2\ 4t_{1u}^6\ 1t_{2g}^6\ 3e_g^4$ x $[1t_{2u}^6\ 5t_{1u}^6]\ 1t_{1g}^6$ [77]
CD_4	T_d	$1a_1^2\ 2a_1^2\ 1t_2^6$ [paper VI]

Table X. Electron configurations of the SF_6 and CD_4 molecules.

SF_6	Type of orbital	Vertical binding energy (eV)	Fragment and its appearance energy
	$1t_2$	15.7	Formation of SF_5^+
	$1t_{2u}$, $5t_{1u}$	17.0	Formation of SF_4^+ at around 18 eV
	$3e_g$	18.7	Formation of SF_4^+
	$1t_{2g}$	19.4	Formation of SF_3^+
	$4t_{1u}$	22.9	Formation of SF_2^+ at around 26 eV
	$5a_{1g}$	26.8	Formation of SF_2^+ [paper VII]

Table XI. The SF_6 outer orbitals studied in this thesis and the appearance energies for the observed fragments SF_n^+ (n = 5-2) [3].

Figure 25 presents a scheme of the ground state SF_6 geometry. The experimental S-F bond equilibrium distance is around 1.55 Å [78]. The fragmentation of SF_6 after valence photo excitation is discussed in paper VII. The ionization energies of the valence orbitals of interest are given in Table XI. The data have been confirmed in our studies presented in paper V and discussed in detail in paper VII. Moreover, our studies reveal the formation of SF_2^+ even after selective ionization of the $5a_{1g}$ orbital. This experimental observation was reported just once before in PEPICO experiments. The lack of experimental observations of this fragment in photoabsorption experiments is most probably due to the very weak partial ionization cross section into this state [79] as is further discussed in section 4.3 and paper VII. The measurements of the CD_4 fragmentation after valence photoexcitation are presented in paper V and discussed in detail for its relevance in different molecular relaxation processes in papers VI and VIII.

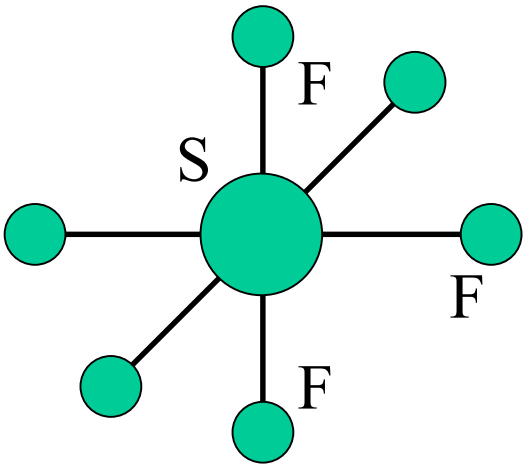

Figure 25. Scheme of the ground state SF_6 geometry.

CD_4	Type of orbital and state term (symmetry)		Vertical binding energy (eV)	Comments
From [43]	$1t_2$	$^2B_1(C_{2v})$	12.43	The $1t_2^{-1}$ state is triply degenerated. Jahn-Teller interaction distorts the molecule to three lower symmetry states. Production of CD_4^+ and CD_3^+
		$^2B_2(D_{2d})$	12.57	
		$^2A_1(C_{3v})$	12.94	
From [80]	$2a_1$	-	22.39	Production of CD_2^+ and CD^+ [paper VI]
From [80]	$1a_1$	-	290.70	Complete CD_4 fragmentation [paper VI]

Table XII. The CD_4 orbitals studied in this thesis, their ionization energies and production of CD_n^+ (n = 4-1) fragments.

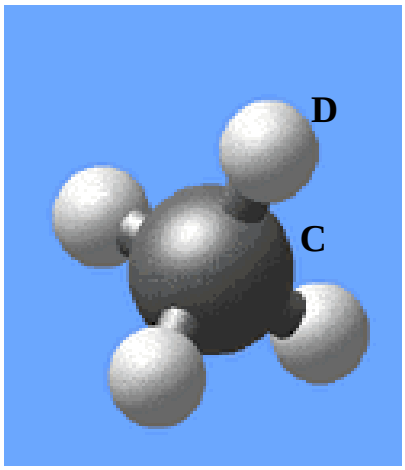

Figure 26. CD_4 ground state geometry.

The ionization energies of the orbitals of interest are given in Table XII above together with the term symbols and symmetries of the $1t_2^{-1}$ valence states and the relevant fragment production observed for each orbital ionization. Figure 26 presents the ground state CD_4 geometry. All the D-C-D

angles are 109.5 degrees and the C-D equilibrium distance is 1.1 Å [9]. All the measurements of the CD_4 fragmentation after photoexcitation are presented in paper V. Papers VI and VIII discuss in detail the measured spectra and propose a model for their explanation. The data in table XII is the basis for the proposed explanation. Papers VI and VIII discuss widely the fragmentation after C 1s ionization and after core excited resonant Auger decay of the CD_4 molecule, respectively. The CD_4^+ relaxation dynamics after the $1t_2$ orbital ionization produce CD_4^+ and CD_3^+ fragments (formation ratio, $CD_3^+/CD_4^+ = 0.8$) until, at excitation energies below C 1s ionization, neutral core excited states are reached. The relaxation from these core-excited states seems to preferentially populate the $^2A_1(C_{3v})$ state responsible for the CD_3^+ fragment production [81] and therefore the formation ratio changes radically up to $CD_3^+/CD_4^+ = 1.33$. The mechanism responsible for this preferential population is still unknown but seems to be the same for all the core-excited states studied since all of them are accessible due to vibronic couplings with vibrational modes of the t_2 symmetry [82]. For excitation energies above C 1s ionization, the fragmentation of the CD_4 molecule is complete, as discussed in detail in paper VI. Sections 4.3 and 4.4 summarize the results obtained in the valence fragmentation studies of SF_6 and CD_4 and the core ionization of CD_4, respectively.

4.1 Neutral dissociation of N_2 and O_2

Neutral dissociation processes have been studied by detecting dispersed fluorescence from excited N and O atoms. In the case of N_2, the excited atoms are created through excitations to members of the molecular Rydberg series of the N_2 molecules, which predissociate. Hence, the following NI fluorescence lines corresponding to the 3p $^4S^0$-3s ^4P, 3p $^4P^0$-3s ^4P, 3p $^4D^0$-3s ^4P and 3p $^2D^0$-3s ^2P atomic transitions are observed. From comparison with calculations using many-body perturbation theory it follows that predissociations of N_2 Rydberg series converging to the C $^2\Sigma_u^+$ and D $^2\Pi_{gi}$ states in N_2^+ are originated by a set of attractive non-Rydberg doubly excited resonances (NRDERs), whose potential curves should be similar to the ones presented in Fig. 5 and Fig. 6 in paper I. The strongest of the predissociation channels observed seems to be mediated by NRDERs of $^1\Sigma_u^-$, $^1\Pi_u$ and $^1\Delta_u$ symmetries leading to the limits 3p $^4P^0$ and 3p $^4D^0$, respectively.

In the case of O_2 the strongest emission occurs from the OI lines corresponding to the atomic transitions 3p ^5P-3s $^5S^0$, 3p ^3P-3s $^3S^0$. Their calculated excitation functions exhibit a line structure which may be attributed to the O_2 Rydberg series R(A), R(b) and R(B). This experimental evidence and the follow up calculations suggest that the neutral photodissociation in the 15-20 eV region occurs after spin-allowed predissociations of the R(A), R(b) and R(B) Rydberg series, mediated by valence states (both singly and doubly excited) with the following triplet symmetries: $^3\Sigma_u^+$, $^3\Sigma_u^-$, $^3\Pi_u$, and $^3\Delta_u$. In the 20.5-25 eV region, emission also occurs from OI (nl) Rydberg states ($n \geq 4$; 4d $^3D^0$-3p ^3P, 5 to

7s $^3S^0$-3p ^3P, 5s $^5S^0$-3p ^5P and 4 to 5d $^5D^0$-3p ^5P) as well as from the 3p $^{3,5}P$ states. Their excitation functions show structures, which partially coincide with those of the O_2 R(c) Rydberg series. No attempt to identify the associated predissociating states is made in view of the high density of states in this region.

4.2 Non Franck-Condon effects in the photoionization of N_2 and O_2

All studied photoionization channels present strong non Franck-Condon effects in their experimental vibrational branching ratios. The photoionization of N_2 molecules to the N_2^+ A $^2\Pi_u$ state has been studied using photoelectron spectroscopy. The performed work is the first systematic experimental and theoretical, vibrational branching ratio study of the photoionization to the N_2^+ A $^2\Pi_u$ state in the 20-34 eV energy region. The spectra show a strong non Franck-Condon feature at around 22 eV. Comparison between experimental data and theoretical *ab initio* computations of the branching ratios reveals that the $2\sigma_u$ shape resonance is not responsible for the observed non Franck-Condon behavior. Excitations to the doubly excited members of the R(C) and R(D) Rydberg series seem to be the origin of the observed features. In addition, excitation to a NRDER of $^1\Sigma^+_u$ symmetry existing at 29.21 eV, with a doubly excited configuration $1\pi_u^2$ $1\pi_g$ $2\pi_u$, and to NRDERs of $^1\Pi_u$ symmetry at 29.26 eV and 28.55 eV respectively, seem to produce the narrow non Franck-Condon structures observed around 28.25 and 29.25 eV.

The photoionization of O_2 molecules to the O_2^+ X $^2\Pi_g$ state has also been studied using photoelectron spectroscopy. The σ_u shape resonance does not influence the ionization to the O_2^+ X $^2\Pi_g$ state. Experimentally, the vibrational branching ratios for the v = 0-3 levels obtained up to 31 eV show a strong previously unobserved Franck-Condon breakdown up to 28 eV. Comparison between *ab initio* computations of vibrational branching ratios (and partial and total cross section for ionization to the X $^2\Pi_g$ state from 15 eV to 60 eV) and theoretical data reveals that the σ_u shape resonance is not the origin of the observed non Frank-Condon effects in the studied region. In addition, excitation to the R(B) and R(c) and perhaps to high vibrational levels of the R(b) Rydberg series and to existing valence states accounts only for some of the structures appearing in the measured branching ratios.

4.3 Valence fragmentation of SF_6 and CD_4

Fragmentation of the SF_6 molecule after excitation with 100 eV synchrotron photons is studied with the EREICO technique, using the new station for multicoincidence experiments recently developed by our group. The mass spectra acquired in coincidence with the ($1t_{1g}$+[$5t_{1u}1t_{2u}$]), ($3e_g$+$1t_{2g}$), $4t_{1u}$ and $5a_{1g}$ electrons reveal strong selectivity in dissociation from these states. Total kinetic energy

released values for candidate reactions producing the observed SF_5^+, SF_4^+ and SF_3^+ fragments are deduced and compared with those existing in the literature obtained with different techniques. Even formation of SF_2^+ after selective ionization of the $5a_{1g}$ orbital is observed, producing a small fraction of very low kinetic energy SF_2^+ fragments. These could be created as follows. Due to the geometry of the SF_6 molecule the SF_2 forms a symmetrical, linear S-F-S core being surrounded by four fluorine atoms lying symmetrically in a perpendicular plane. In the proposed scenario, this core is left almost stationary and the ejected fluorine atoms take the excess energy.

Fragmentation of the CD_4 molecule after excitation with 70 eV synchrotron photons is studied for the first time with the EREICO technique. The mass spectra acquired in coincidence with the $1t_2$ electrons reveal production of CD_4^+ and CD_3^+ fragments (formation ratio, $CD_3^+/CD_4^+ = 0.8$) only. These fragments are produced after dissociations from the three possible $1t_2^{-1}$ CD_4^+ Jahn-Teller distorted states $^2B_1$ (of C_{2v} symmetry), $^2B_2$ (of D_{2d} symmetry) and $^2A_1$ (of C_{3v} symmetry). For the $2a_1^{-1}$ state only the D^+, CD^+ and CD_2^+ fragments are observed. The parent CD_4^+ ion formed is always unstable and does not dissociate into CD_3^+ fragments. This is correlated with a similar strong coupling to the dissociation continuum in methane. At the $2a_1^{-1}$ threshold, H^+ and CH^+ appear and there is also production of CH_2^+. The CH_3^+ fragment is either not formed in predissociation of the $2a_1^{-1}$ state or is subject to further decay processes. One of the possible mechanisms for the production of CH_2^+ could be predissociation of the $2a_1^{-1}$ state by the repulsive states of $^2A_1$ (of C_{2v} symmetry) computed in the energy region of the $2a_1^{-1}$.

4.4 Fragmentation of CD_4 below and above C 1s ionization

The fragmentation studies of CD_4 below and above C 1s ionization have been performed also for the first time using EREICO measurements. Below C 1s ionization, relaxation via participator Auger decay from several core-excited states has been monitored. A summary of the obtained results is presented in section 4.4.1 and in paper VIII. The results of the studies above the C1s ionization of the CD_4 molecule are presented in section 4.4.2 and paper VI.

4.4.1 Below C 1s ionization

Selective excitation of the C $1s(1a_1) \rightarrow 3sa_1$ and C $1s(1a_1) \rightarrow 3pt_2$ and $3pt_2$ + v Rydberg transitions produce CD_3^+ and CD_4^+ fragments. The production of CD_3^+ is enhanced up to 68% after C 1s excitation to different core excited states with respect to the ratio observed after direct ionization of the $1t_2$ orbital. This enhancement is correlated with the different geometrical and dynamical changes that the molecule experiences when relaxing via participator Auger decay from the core-excited states.

These changes seem to favor the decay to the CD_4^+ $^2A_1(C_{3v})$ state over the other possible states of the CD_4^+ ground state ion through different relaxation mechanisms depending on the core-excited state they decay from. From this state, the CD_4^+ is energetically allowed to undergo dissociation into CD_3^+ + D. The mechanism responsible for this preferential population is still unknown but seems to be the same for all the core-excited states studied since all the core excited states studied are accessible due to vibronic couplings with vibrational modes of the t_2 symmetry. These results are the first experimental evidence of core-excited induced dissociation in the CD_4 molecule.

4.4.2 Above C 1s ionization

The photoionization of the C 1s ($1a_1$) core orbital by 350 eV photons reveals a rich fragmentation pattern, compared to those patterns obtained after outer and inner valence orbital photoionization. The C 1s ionization is followed by electronic Auger decay creating CD_4^{2+}. This relaxation mechanism causes a more complete fragmentation of the molecule than the direct valence photoionization. The study reveals that carbon core ionization opens new photodissociation pathways not available in the valence ionization regime. With the aid of ab initio quantum chemistry calculations, a two-step model of the dissociation following normal Auger decay after carbon core ionization is proposed. The CD_4^{2+} molecule first undergoes dissociation into $CD_3^+ + D^+$. This process converts a large amount of potential energy into translational and vibrational energy of the fragments. Thus, in some cases the vibrational energy of the CD_3^+ fragment is enough to produce a secondary dissociation creating CD_2^+, CD^+ and C^+ fragments, as experimentally detected. The translational kinetic energy computed for these lighter fragments from the experimental mass spectra is progressively smaller. This is accounted for in the proposed model since more of the available energy is used as vibrational energy to further dissociate the CD_3^+ fragment. This sequential dissociation scenario presented is an alternative to the simultaneous multiparticle dissociation scenario.

References

[1] P. S. Zurer, *Antarctic ozone hole: complex picture emerges.* Chem. & Engin. News **65**, (1987) 22.

[2] D. Wade, *Deuterium isotope effects on noncovalent interaction between molecules.* Chem.-Bio. Inter. **117**, (1999) 191.

[3] L. G. Christophorou and J. K. Olthoff, *Electron interactions with SF_6.* J. Phys. Chem. Ref. Data **29**, (2000) 267.

[4] P. Erman, A. Karawajczyk, U. Köble, E. Rachlew-Källne, K. Yoshiki Franzén and L. Veseth, *Ultrashort-lived non-Rydberg doubly excited resonances observed in molecular photoionization*. Phys. Rev. Lett. **76,** (1996) 4136.

[5] G. Wendin, *Collective effects, relaxation and localization of hole levels in atoms, molecules, solids and adsorbates*. Int. J. Q. Chem.: Q. Chem. Symp. **13,** (1979) 659.

[6] M. Ukai, S. Machita, K. Kamela, M. Kitajima, N. Kouchi Y. Hatano and K. Ito, *State-to-state behavior in the neutral dissociation of O_2 far beyond the ionization threshold*. Phys. Rev. Lett. **74,** (1995) 239.

[7] P. Erman, A. Karawajczyk, E. Rachlew-Källne, M. Stankiewicz, K. Yoshiki Franzén, P. Sannes and L. Veseth, *Ultrashort-lived non-Rydberg doubly excited resonances in diatomic molecules*. Phys. Rev. A **55,** (1997) 4221.

[8] Y. Hatano, *Interaction of VUV photons with molecules. Spectroscopy and dynamics of molecular superexcited states.* J. Elec. Spectr. Rel. Phenom. **119**, (2001) 107.

[9] T. Odagiri, K. Takahashi, K. Yoshikawa, N. Kouchi and Y. Hatano, *Forbidden doubly excited states of molecular nitrogen dissociating into two neutral atoms in electron collisions.* J. Phys. B: At. Mol. Opt. Phys. **34**, (2001) 4889.

[10] R. Flammini, E. Fainelli, L. Avaldi, *Observation of doubly excited states in the N_2^+ $2\sigma_u^{-1}$ partial ionization cross sections measured by (e, 2e) experiments.* J. Phys. B: At. Mol. Opt. Phys. **33**, (2000) 1507.

[11] M. Neeb, A. Kivimäki, B. Kempgens, H. M. Köppe, J. Feldhaus and A. M. Bradshaw, *Core hole double-excitation and atomic like Auger decay in N_2.* Phys. Rev. Lett. **76**, (1996) 2250.

[12] S. S. Tayal, *Resonant photoionization cross sections and intensity ratios for atomic oxygen*. Phys. Rev. A **65,** (2002) 03724.

[13] S. N. Nahar, *Photoionization cross sections and oscillator strengths for oxygen ions: O_I-O_{VII}.* Phys. Rev. A **58**, (1998) 3766.

[14] A. F. Goncharov, E. Gregoryanz, H. K. Mao, Z. Liu and R. J. Hemley, *Optical evidence for a nonmolecular phase of nitrogen above 150 GPa.* Phys. Rev. Lett. **85**, (2000) 1262.

[15] J. Liu, R. Li, Z. Xu and J. Liu, *Approximately analytical model for inner-shell photoionization x-ray lasers in low-Z elements.* Phys. Rev. A **63**, (2001) 033809.

[16] U. Becker, O. Gessner and A. Rüdel, *Photoelectron scattering in molecules and fullerenes.* J. Elec. Spectr. Rel. Phenom. **108**, (2000) 189.

[17] K. Ueda, M. Simon, C. Miron, N. Leclercq, R. Guillemin, P. Morin and S. Tanaka, *Correlation between nuclear motion in the core-excited CF_4 molecule and molecular dissociation after resonant Auger decay.* Phys. Rev. Lett. **83**, (1999) 3800.

[18] L. Vial, A. M. Casanovas, J. Diaz, I. Coll and J. Casanovas, *Decomposition of high-pressure (400kPa) SF6 and Sf6/N2 (10:90) mixtures submitted to negative or 50 Hz ac corona discharges in the presence of water vapor and/or oxygen*. J. Phys. D: Appl. Phys. **34**, (2001) 2037.

[19] T. Ogawa, K. Mochiji, I. Ochiai, S. Yamamoto and K. Tanaka, *Low temperature synchrotron-radiation-excited etching of silicon dioxide with sulfur hexafluoride adsorption*. J. Appl. Phys. **75**, (1994) 4680.

[20] J. Yoshinobu, H. Ogasawara and M. Kawai, *Symmetry controlled surface photochemistry of methane on Pt (111)*. Phys. Rev. Lett. **75**, (1995) 2176.

[21] L. B. F. Juurlink, P. R. McCabe, R. R. Smith, C. L. DiCologero and A. L. Utz, *Eigenstate-resolved studies of gas-surface reactivity: CH_4 (ν_3) dissociation on Ni(100).* Phys. Rev. Lett. **83**, (1999) 868.

[22] J. D. Kress, S. R. Bickham, L. A. Collins, B. L. Holian, and S. Goedecker, *Tight-binding molecular dynamics of shock waves in methane.* Phys. Rev. Lett. **83**, (1999) 3896.

[23] A. S. Barabash, S. G. Belogurov, V. N. Kornoukhov, V. F. Kuzichev, V. N. Stekhanov, *Liquid deuteromethane pulse ionization chamber.* Nucl. Instrum. Meth. Phys. Res. A **434,** (1999) 478.

[24] I. Nenner and J. A. Beswick, *Handbook of synchrotron radiation vol. 2. Molecular photodissociation and photoionization.* Elsevier Science, (1987).

[25] G. Herzberg, *Molecular spectra and molecular structure. Spectra of diatomic molecules.* **I** Krieger, Florida (1950).

[26] I. N. Levine, *Quantum chemistry.* Prentice Hall, New York (2000).

[27] J. J. Sakurai, *Modern quantum mechanics.* Addison-Wesley, New York (1994).

[28] P. W. Atkins, *Physical chemistry. 5th ed*. Oxford University Press, Oxford (1994).

[29] M. Karplus and R. N. Porter, *Atoms & molecules. An introduction for students of physical chemistry.* W. A. Benjamin Inc., London (1970).

[30] J. Franck, *Elementary processes of photochemical reactions*. Trans. Farad. Soc. **21**, (1925) 536.

[31] E. U. Condon, *Nuclear motions associated with electron transitions in diatomic molecules*. Phys. Rev. **32**, (1928) 858.

[32] M. Ukai, K. Kameta, N. Kouchi, Y. Hatano and K. Tanaka, *Neutral decay of double-holed doubly excited resonances of N_2.* Phys. Rev. A **46**, (1992) 7019.

[33] L. Veseth, *Method to compute atomic and molecular photoionization cross sections by use of basis sets.* Phys. Rev. A. **44**, (1991) 358.

[34] L. Veseth, *Many-body calculation of total and partial photoabsorption cross sections in N_2.* J. Phys. B: At. Mol. Opt. Phys. **27**, (1994) 481.

[35] L. Veseth, *Many-body calculation of autoionization rates in atoms and molecules.* J. Phys. B: At. Mol. Opt. Phys. **29**, (1996) 977.

[36] P. Sannes and L. Veseth, *Doubly excited autoionizing states in N_2.* Phys. Rev. A **56**, (1997) 2893.

[37] P. Erman, A. Karawajczyk, E. Rachlew-Källne, S.L. Sorensen and C. Strömholm, *Synchrotron radiation induced photoionization and photodissociation of small molecules.* J. de Physique IV **C9**, (1993) 393.

[38] P. Erman, A. Karawajczyk, E. Rachlew-Källne, M. Stankiewicz and K. Yoshiki Franzén, *Energy distributions of O^+ ions produced in photodissociation of O_2 in the 17-34 eV range.* J. Phys. B: At. Mol. Opt. Phys. **29**, (1996) 5785.

[39] P. Erman and E. Rachlew-Källne, *The use of synchrotron radiation in atomic and molecular physics.* Kompendium, Institutionen för Fysik I, KTH (1996).

[40] J.-H. Fock and E. E. Koch, *Shape resonances and partial photoemission cross sections of solid SF_6 and CCl_4.* Chem. Phys. **96**, (1985) 125.

[41] G. Herzberg, *The spectra and structures of simple free radicals. An introduction to molecular spectroscopy.* Cornell University Press, London (1971).

[42] H. A. Jahn and E. Teller, *Stability of polyatomic molecules in degenerate electronic states.* Proc. Roy. Soc. A **161**, (1937) 220.

[43] K. Takeshita, *A theoretical analysis of the Jahn-Teller effect in the photoelectron spectrum of methane*. J. Chem. Phys. **86**, (1987) 329.

[44] E. Kukk, J. Rius i Riu, M. Stankiewicz, P. A. Hatherly, P. Erman, E. Rachlew-Källne, P. Winiarczyk, M. Huttula and S. Aksela. *Dissociation of deuteromethane following carbon 1s core ionization*. Phys. Rev. A **66**, (2002) 012704.

[45] P. Auger, J. de Physique (Paris) **6**, (1925) 205.

[46] S. Sundin, *Photoelectron spectroscopy in the vicinity of a core-ionization threshold*. Doctoral Thesis, Acta Univer. Upsalien. **397**, Uppsala (1998).

[47] J. L. Dehmer and D. Dill, *Shape resonances in K-shell photoionization of diatomic molecules.* Phys. Rev. Lett. **35,** (1975) 213.

[48] J. L. Dehmer, D. Dill and Scott Wallace, *Shape-resonances-enhanced nuclear-motion effects in molecular photoionization.* Phys. Rev. Lett. **43,** (1979) 1005.

[49] L.D. Landau and E. M. Lifshitz, *Statistical physics. 3rd ed.* Pergamont, Oxford (1980).

[50] A. Lofthus and P. H. Krupenie, *The spectrum of molecular nitrogen.* J. Phys. Chem. Ref. Data **6,** (1977) 113.

[51] P. H. Krupenie, *The spectrum of molecular oxygen.* J. Phys. Chem. Ref. Data **1,** (1972) 423.

[52] L.-E. Berg, P. Erman, E. Källne, S. Sorensen and G. Sundström, *Studies of photoionization and photodissociation of N_2 in the 15-30 eV region using intense synchrotron radiation.* Physica Scripta **44,** (1991) 131.

[53] P. Erman, A. Karawajczyk, E. Rachlew-Källne, S. L. Sorensen and C. Strömholm, *Visible and VUV fluorescence from synchrotron radiation induced photoionization and photodissociation of molecular oxygen.* Physica Scripta **49,** (1994) 308.

[54] T. H. Dunning Jr., *Gaussian basis sets for use in correlated molecular calculations. I. The atoms boron through neon and hydrogen.* J. Chem. Phys. **90**, (1989) 1007.

[55] *Dalton, a molecular electronic structure program*, Release **1.2,** (2001), written by T. Helgaker, H. J. A. Jensen, P. Jørgensen, J. Olsen, K. Ruud, H. Ågren, A. A. Auer, K. L. Bak, V. Bakken, O. Christiansen, S. Coriani, P. Dahle, E. K. Dalskov, T. Enevoldsen, B. Fernandez, C. Hättig, K. Hald, A. Halkier, H. Heiberg, H. Hettema, D. Jonsson, S. Kirpekar, R. Kobayashi, H. Koch, K. V. Mikkelsen, P. Norman, M. J. Packer, T. B. Pedersen, T. A. Ruden, A. Sanchez, T. Saue, S. P. A. Sauer, B. Schimmelpfennig, K. O. Sylvester-Hvid, P. R. Taylor and O. Vahtras, computer code DALTON, http://www.kjemi.uio.no/software/dalton/dalton.html

[56] J. N. Andersen, R. Nyholm and S. L. Sorensen, *MAX LAB activity report*. (1999) 29.

[57] E. Koch, D.E. Eastman and Y. Farge, *Handbook of synchrotron radiation*. **1,** North Holland, Amsterdam (1983).

[58] H. Winick, *Synchrotron radiation sources: a primer*. Series on Synchrotron Radiation Techniques and Applications. **1,** World Scientific, London (1994).

[59] S. L. Sorensen, B. J. Olsson, O. Widlund, S. Huldt, S.-E. Johansson, E. Källne, A. E. Nilsson, R. Hutton, U. Litzén and A. Svensson, *A normal-incidence beam line at the MAX storage ring.* Nucl. Instr. and Meth. in Phys. Research A **297,** (1990) 296.

[60] K. Yoshiki Franzén, *Formation and fragmentation dynamics of superexcited molecules*. Doctoral Thesis, The Royal Institute of Technology KTH, Stockholm (1998).

[61] M. Bässler, J. -O. Forsell, O. Björneholm, R. Feifel, M. Jurvansuu, S. Aksela, S. Sundin, S. L. Sorensen, R. Nyholm, A. Ausmees and S. Svensson, *Soft x-ray undulator beam line I411 at MAX-II for gases, liquids and solids samples.* J. Electron Spectrosc. **101-103**, (1999) 953.

[62] S. Svensson, J.-O. Forsell, H. Siegbahn, A. Ausmees, G. Bray, S. Södergren, S. Sundin, S. J. Osborne, S. Aksela, E. Nõmmiste, J. Jauhiainen, M. Jurvansuu, J. Karvonen, P. Barta, W. R.

Salaneck, A. Evaldsson, M. Lögdlund and A. Fahlman, *New end station for the study of gases, liquids and solid films at the MAX laboratory.* Rev. Sci. Instrum. **67**, (1996) 2149.

[63] Jobin Yvon Spex, *Guide for spectroscopy.* Instruments S. A. Group (1994).

[64] W. R. Leo, *Techniques for nuclear and particle physics experiments.* 2nd Ed. Springer-Verlag (1994).

[65] Omicron Instruments for Surface Science, *EA 125 Energy analyser technical reference manual.* Omicron Vakuumphysik (1997).

[66] R. N. Zare. *Photoejection dynamics [1].* Mol. Photochem. **4,** (1972) 1.

[67] W. C. Wiley and I. H. McLaren. *Time-of-flight mass spectrometer with improved resolution.* Rev. Sci. Instrum. **26**, (1955) 1150.

[68] P. Erman, A. Karawajczyk, E. Rachlew-Källne, S. L. Sorensen, C. Strömholm and M. Kirm. *Studies of fluorescence from photoionization and photodissociation of N_2 induced by 16-40 eV synchrotron radiation*. J. Phys. B **26,** (1993) 4483.

[69] J. Cruyff, *Barça 5 - Real Madrid 1.* Press Conference after the Game, Barcelona (1992).

[70] P. Winiarczyk. *Relaxation of highly excited molecules studied with charged particle spectroscopies*. Doctoral Thesis, Instytut Fizyki im. Mariana Smoluchowskiego, Uniwersytet Jagielloński, Krakow (2002).

[71] C. Nordling and J. Österman. *Physica handbook, elementary constants and units tables, formulae and diagrams and mathematical formulae.* Studentlitteratur, Lund, (1987).

[72] P. Baltzers, M. Larsson, L. Karlsson, B. Wannberg and M. Carlsson Göthe, *Inner-valence states of N_2^+ studied by UV photoelectron spectroscopy and configuration-interaction calculations.* Phys. Rev. A **46**, (1992) 5545.

[73] P. Baltzers, B. Wannberg, L. Karlsson, M. Carlsson Göthe and M. Larsson, *High-resolution inner-valence UV photoelectron spectra of the O_2 molecule and configuration-interaction calculations of $^2\Pi_u$ states between 20 and 26 eV.* Phys. Rev. A **45**, (1992) 4374.

[74] H. Liebel, A. Ehresmann, H. Schmoranzer, Ph. V. Demekhin, B. M. Lagutin and V. L. Sukhorukov. *De-excitation dynamics of Rydberg states in O_2: I. Total cross sections for OI fluorescence emission following predissociation of $2\sigma_u^{-1}$ ($c\ ^4\Sigma_u^-$) $n\sigma_g\ ^3\Sigma_u^-$ states*. J. Phys. B: At. Mol. Opt. Phys. **35**, (2002) 895.

[75] A. C. Parr, J. B. West, G. V. Marr and J. L. Dehmer, *Evidence derived from angle-resolved electron spectroscopy for a new spectral series in he photoionization continuum of molecular oxygen*. J. Phys. B: At. Mol. Opt. Phys. **31**, (1998) 5161.

[76] G. Öhrwall, P. Baltzer and J. Bozek, *Photoelectron spectra of N_2^+: rotational line profiles studied with He I-excited angle-resolved spectroscopy and with synchrotron radiation*. Phys. Rev. A **59**, (1999) 1903.

[77] T. Gustafsson, *Partial photoionization cross sections of SF6 between 20 and 54 eV: an interpretation of the photoelectron spectrum*. Phys. Rev A. **18**, (1978) 1481.

[78] H. Tachikawa, *Ab initio MO calculations of structures and electronic states of SF_6 and SF_6^-*. J. Phys. B: At. Mol. Opt. Phys. **35**, (2002) 55.

[79] J. C. Creasey, I. R. Lambert, R. P. Tuckett, K. Codling, L. Frasinski, P. A. Hatherly and M. Stankiewicz, *Fragmentation of valence electronic states of SF_6^+ studied with synchrotron radiation*. J. Chem. soc. Faraday Trans. **87**, (1991) 1287.

[80] S. L. Sorensen, A. Karawajczyk, C. Strömholm and M. Kirm. *Dissociative photo excitation of CH_4 and CD_4*. Chem. Phys. Lett. **232**, (1995) 554.

[81] E. F. van Dishoeck, W. J. van der Hart and M. van Hemert, *Ab initio studies of the photodissociation processes in positive hydrocarbons ions. I. The methane ion*. Chem. Phys. **50**, (1980) 45.

[82] A. B. Rocha and C. E. Bielschowsky. *Isotopic effects in inner-shell spectrum of methane: a theoretical study*. J. Mol. Struc. (Theochem) **539**, (2001) 145.